Pharmacological Research 190 (2023) 106724

Contents lists available at ScienceDirect

Pharmacological Research

journal homepage: www.elsevier.com/locate/yphrs

Organic anion-transporting polypeptide 2B1 knockout and humanized mice; insights into the handling of bilirubin and drugs

Wenlong Li [a,1], Dilek Iusuf [a], Rolf W. Sparidans [b], Els Wagenaar [a], Yaogeng Wang [a], Dirk R. de Waart [c], Margarida L.F. Martins [a], Stéphanie van Hoppe [a], Maria C. Lebre [a], Olaf van Tellingen [a], Jos H. Beijnen [a,d,e], Alfred H. Schinkel [a,*]

[a] The Netherlands Cancer Institute, Division of Pharmacology, Plesmanlaan 121, 1066 CX Amsterdam, the Netherlands
[b] Utrecht University, Faculty of Science, Department of Pharmaceutical Sciences, Division of Pharmacology, Universiteitsweg 99, 3584 CG, Utrecht, the Netherlands
[c] Tytgat Institute for Liver and Intestinal Research, Academic Medical Center, Meibergdreef 71, 1105 BK, Amsterdam, the Netherlands
[d] Utrecht University, Faculty of Science, Department of Pharmaceutical Sciences, Division of Pharmacoepidemiology & Clinical Pharmacology, Universiteitsweg 99, 3584 CG Utrecht, the Netherlands
[e] The Netherlands Cancer Institute, Department of Pharmacy & Pharmacology, Plesmanlaan 121, 1066 CX Amsterdam, the Netherlands

ARTICLE INFO

Keywords:
Organic anion-transporting polypeptide 2B1
Genetically modified mouse models
Bilirubin
Drug disposition
Oral availability
Tissue distribution

Chemical compounds studied in this article:
Bilirubin (PubChem CID: 5280352)
Bilirubin diglucuronode (PubChem CID: 5280817)
Erlotinib (PubChem CID: 176870)
OSI-420 (10317566)
OSI-413 (PubChem CID: 18925012)
Pravastatin (PubChem CID: 54687)
Rosuvastatin (PubChem CID: 446157)
Fluvastatin (PubChem CID: 446155)
Fexofenadine (PubChem CID: 3348)

ABSTRACT

Organic anion transporting polypeptide 2B1 (OATP2B1/*SLCO2B1*) facilitates uptake transport of structurally diverse endogenous and exogenous compounds. To investigate the roles of OATP2B1 in physiology and pharmacology, we established and characterized Oatp2b1 knockout (single *Slco2b1*$^{-/-}$ and combination *Slco1a/1b/2b1*$^{-/-}$) and humanized hepatic and intestinal OATP2B1 transgenic mouse models. While viable and fertile, these strains exhibited a modestly increased body weight. In males, unconjugated bilirubin levels were markedly reduced in *Slco2b1*$^{-/-}$ compared to wild-type mice, whereas bilirubin monoglucuronide levels were modestly increased in *Slco1a/1b/2b1*$^{-/-}$ compared to *Slco1a/1b*$^{-/-}$ mice. Single *Slco2b1*$^{-/-}$ mice showed no significant changes in oral pharmacokinetics of several tested drugs. However, markedly higher or lower plasma exposure of pravastatin and the erlotinib metabolite OSI-420, respectively, were found in *Slco1a/1b/2b1*$^{-/-}$ compared to *Slco1a/1b*$^{-/-}$ mice, while oral rosuvastatin and fluvastatin behaved similarly between the strains. In males, humanized OATP2B1 strains showed lower conjugated and unconjugated bilirubin levels than control Slco1a/1b/2b1-deficient mice. Moreover, hepatic expression of human OATP2B1 partially or completely rescued the impaired hepatic uptake of OSI-420, rosuvastatin, pravastatin, and fluvastatin in *Slco1a/1b/2b1*$^{-/-}$ mice, establishing an important role in hepatic uptake. Expression of human OATP2B1 in the intestine was basolateral and markedly reduced the oral availability of rosuvastatin and pravastatin, but not of OSI-420 and fluvastatin. Neither lack of Oatp2b1, nor overexpression of human OATP2B1 had any effect on fexofenadine oral pharmacokinetics. While these mouse models still have limitations for human translation, with additional work we expect they will provide powerful tools to further understand the physiological and pharmacological roles of OATP2B1.

Abbreviations: ABC, ATP-binding cassette; ANOVA, analysis of variance; AUC, area under plasma concentration-time curve; BAC, bacterial artificial clone; BBB, blood-brain barrier; BDG, bilirubin diglucuronide; BMG, bilirubin monoglucuronide; C_{max}, maximum drug concentration in plasma; CYP, Cytochrome P450; LC-MS/MS, liquid chromatography coupled with tandem mass spectrometry; OATP, organic anion-transporting polypeptides; SD, standard deviations; *Slco1a/1b/2b1*$^{-/-}$, Slco1a/1b/2b1 knockout mice; Slco12B1-Apo, Slco1a/1b/2b1 knockout mice with specific expression of human SLCO2B1 in liver; Slco12B1-Vil, Slco1/1b/2b1 knockout mice with specific expression of human SLCO2B1 in intestine; T_{max}, time to reach maximum drug concentration in plasma; UCB, unconjugated bilirubin; Ugt1a1, UDP-glucuronosyltransferase 1a1.

* Correspondence to: Division of Pharmacology, The Netherlands Cancer Institute, Plesmanlaan 121, 1066 CX Amsterdam, the Netherlands.
E-mail address: a.schinkel@nki.nl (A.H. Schinkel).
[1] Present address: Cancer Research UK Cambridge institute, University of Cambridge, Li Ka Shing Centre, Robinson Way, Cambridge CB2 0RE, United Kingdom.

https://doi.org/10.1016/j.phrs.2023.106724
Received 17 January 2023; Received in revised form 25 February 2023; Accepted 9 March 2023
Available online 11 March 2023

1. Introduction

Organic anion transporting polypeptides (human: OATP, gene: *SLCO*; rodent: Oatp, gene: *Slco*) belong to the superfamily of the solute carrier class (SLC) of organic anion transporters [1]. These transporters are involved in sodium-independent cellular uptake of a wide variety of both organic endogenous and exogenous compounds [2,3]. OATP subfamilies are thought to play a vital role in drug disposition due to this broad substrate specificity, and their expression in pharmacokinetically important tissues [4,5].

OATP2B1, initially referred to as OATP-B, was originally cloned from human brain tissue [6,7]. It is one of the main members of the human OATP family, along with OATP1B1 and OATP1B3. In contrast to the liver-specific expression of OATP1B1 and OATP1B3, OATP2B1 has a wider expression profile, including liver, small intestine, kidney, heart, placenta, skeletal muscle, macrophage, and blood-brain barrier (BBB) [8]. The broad tissue distribution of OATP2B1 and its substrate poly-specificity have led to much speculation about its role in the liver uptake of compounds, the intestinal absorption of drugs, the distribution of drugs to various tissues, as well as the BBB penetration of drugs [8]. Moreover, OATP2B1 has been identified in multiple tumor cell lines, and the abundance of the transporter increases with tumor grade [9,10]. This increase may indicate that OATP2B1 is involved in tumor progression perhaps by facilitating the uptake of hormones and steroid sulfates such as estrone sulfate (E3S) [11]. Furthermore, OATP2B1 could mediate macrophage uptake of indoxyl sulfate, resulting in accelerated atherogenesis in chronic kidney disease *via* triggering the Dll4-Notch signaling pathway [12].

In spite of this expression pattern, the functional evidence for hepatic and intestinal OATP2B1-mediated uptake is limited, and the magnitude of its possible impact on oral absorption is not very clear from the literature. Described OATP2B1 substrates frequently have limited supporting *in vitro* data and often demonstrate only modest differences between transporter and control conditions [13,14]. The proposed pharmacokinetic impact of OATP2B1 has largely been derived from drug-drug and food-drug interaction studies [8], but food additive (colorant)/fruit juice interactions are ill-defined due to their complex and incompletely defined composition. Moreover, drug interactions may not only be limited to OATP2B1 but may reflect other contributing factors, such as osmolality effects, as recently shown for the previously reported OATP2B1 substrate atenolol [15]. Additionally, many of the intestinal drug interactions attributed to OATP2B1 have demonstrated only modest effects [8], and often the hepatic drug interactions are not limited to OATP2B1 [16,17].

The hepatic expression level of OATP2B1 is of the same order as that of OATP1B1 and − 1B3 based on proteomics data, suggesting that OATP2B1 is involved directly in liver uptake and indirectly in biliary excretion of xenobiotic substrates [18,19]. However, because there is a significant overlap in the substrate specificity of OATP2B1 with other hepatic OATPs [8,20], the actual independent contribution of OATP2B1 to liver uptake of compounds remains unknown. Another potentially confusing observation showed that OATP2B1 may be primarily localized in the basolateral rather than the apical (luminal) membrane of enterocytes, as was originally reported [21,22]. These paradoxical findings indicate that intestinal OATP2B1 may not only play a role in absorption of compounds from the gut lumen, as has historically been assumed, but also in the removal of some substrates from the blood circulation.

Very recently, a mouse model in C57BL/6 N background lacking Oatp2b1 transporter activity was generated and used to study the role of Oatp2b1 in plasma exposure of drugs, including fluvastatin, rosuvastatin, and fexofenadine [23,24]. In this *Oatp2b1*$^{-/-}$ strain, plasma exposure of orally administered fluvastatin was substantially reduced compared to wild-type mice, suggesting that Oatp2b1 could mediate intestinal fluvastatin absorption. However, in these mice, no effect was observed on rosuvastatin pharmacokinetics, despite robust *in vitro* mouse (m) Oatp2b1-mediated transport of the compound in the same study [24].

This study aimed to increase our knowledge of the physiological and pharmacological roles of the OATP2B1 transporter *in vivo*. To achieve this goal, firstly, we generated and characterized single *Slco2b1*$^{-/-}$ mice. Considering that mOatp1a/1b and mOatp2b1 transporters display a large overlap in tissue distribution and substrate specificity and that mOatp1a/1b transporters frequently play a dominant role in the pharmacokinetics of drugs, we then developed and characterized a mouse model that is functionally deficient for all *Slco1a*, *Slco1b*, and *Slco2b1* genes to better investigate the roles of the Oatp2b1 transporter by comparing to Slco1a/1b knockout mice [25]. Furthermore, OATP2B1 transgenic mice specifically overexpressing the human OATP2B1 transporter in liver or intestine were generated and characterized to assess the roles of the human OATP2B1 transporter. We then used these mouse models to analyze the *in vivo* influence of mOatp2b1 and hOATP2B1 on the disposition of several compounds to better understand their possible relevance in the pharmacokinetics of drugs.

2. Materials and methods

2.1. Chemicals and reagents

Erlotinib and rosuvastatin were purchased from TargetMol (Boston, MA, USA). Fluvastatin, fexofenadine, and OSI-420 (desmethyl erlotinib) were obtained from MedChem Express (Middle County, USA). Pravastatin sodium was from Sequoia Research Products (Pangbourne, United Kingdom). Bovine Serum Albumin (BSA) fraction V was from Roche Diagnostics (Mannheim, Germany). Isoflurane was purchased from Pharmachemie (Haarlem, The Netherlands), and heparin sodium (5000 IU/ml) was from Leo Pharma BV (Breda, The Netherlands). All other chemicals and reagents were obtained from Sigma-Aldrich (Steinheim, Germany).

2.2. Construction of targeting vectors for generation of *Slco2b1*$^{-/-}$ mice

The genomic DNA encoding exons 1–6 (out of a total of 13) of the *Slco2b1* gene was isolated from a bacterial artificial clone (BAC) and subcloned into a pGEM5zf+ vector. A reversed PGK-hygromycin cassette was inserted to replace exon 3 and some surrounding intronic regions and the last nucleotides of exon 2, leading to a frameshift (Fig. 1A). A linearized fragment from this construct was used for electroporation into E14 embryonic stem cells. Homologous recombination was checked by enzymatic digestion using *Spe*I, which resulted in a 4.9 kb (5′) and a 7.6 kb (3′) fragment instead of the endogenous 13.1 kb fragment. The probes used were situated outside the linearized fragment. A third check was done with a specific hygromycin-probe.

2.3. Generation of *Slco2b1*$^{-/-}$ and *Slco1a/1b/2b1*$^{-/-}$ mice

Chimeric mice were generated by microinjection of 2 independently targeted ES clones with the Slco2b1 disruption (with the correct karyotype) into blastocysts derived from C57BL/6 J mice. Subsequently, these blastocysts were implanted into the oviducts of pseudo-pregnant F1 fosters (C57BL/6 J mice), which carried them to term. Crossbreeding of resulting germline transmission *Slco2b1*$^{+/-}$ chimeric mice with FVB/N mice yielded 2 independent *Slco2b1*$^{-/-}$ mouse lines.

Homozygous combination knockout mice lacking all *Slco1a/1b* and *Slco2b1* genes were obtained by crossing previously described Slco1a/1b knockout mice [25] with Slco2b1 knockout mice.

Quantitative reverse transcription PCR (RT-qPCR) was applied to initially validate the knockout of Slco2b1 at the RNA level in *Slco2b1*$^{-/-}$ and *Slco1a/1b/2b1*$^{-/-}$ mouse strains using the commercial Slco2b1 (Mm_Slco2b1_1_SG QuantiTect Primer Assay, QT00105728) and β-actin (housekeeping gene; Mm_Actb_1_SG QuantiTect Primer Assay, QT00095242) primers. The delta-delta Ct method was used to normalize the data.

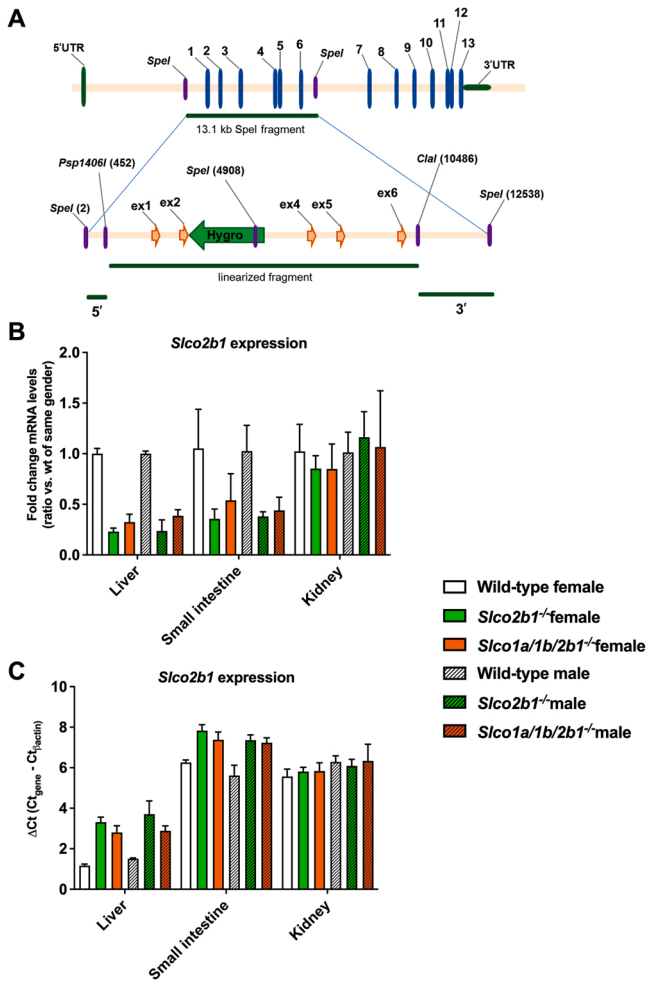

Fig. 1. Generation of *Slco2b1*$^{-/-}$ mice. (A) Disruption of the *Slco2b1* gene. The genomic DNA encoding exons 1–6 (out of a total of 13) of the *Slco2b1* gene was isolated from a bacterial artificial clone (BAC) and subcloned into a pGEM5zf+ vector. A reversed PGK-hygromycin cassette was inserted to replace exon 3 and some surrounding intronic regions and the last nucleotides of exon 2, leading to a frameshift. (B and C) RT-PCR analysis of *Slco2b1* gene expression in liver, small intestine, and kidney of wild-type, *Slco2b1*$^{-/-}$, and *Slco1a/1b/2b1*$^{-/-}$ mice. UTR: untranslated region. Ex: exon. Hygro: hygromycin.

2.4. Generation of Slco12B1-Apo and Slco12B1-Vil mice

The template, human *SLCO2B1* cDNA (accession NM_007256.5), was a kind gift from Dr. R.B. Kim (Western University, London, Ontario, Canada). Liver-specific expression of the human *SLCO2B1* cDNA was achieved by generating the following transgene constructs. pLiv-LE.6 (kindly provided by Dr. J. Taylor, University of California, San Francisco, CA) containing the human ApoE promoter region (including exon 1, intron 1, and partial exon 2 of ApoE) was completely cut with *Cla*I, followed by partial cutting with *Asp*718. The right-sized fragment was isolated by gel electrophoreses, cut out, and purified with Qiaexll gel purification kit (Qiagen). The 3′ and 5′ ends of this vector were filled up with Klenow enzyme to create blunt ends, followed by blunt-end ligation (closure of the vector). The *Xho*I (unique) site was cut open, the ends were filled in with Klenow and treated with CIP, which was used as a vector for ligation of *SLCO2B1* cDNA. Human *SLCO2B1* cDNA was released as an *Xba*I/*Spe*I 2.2 kb fragment from pEF6/V5-HIS-TOPO-SLCO2B1 and blunt-ended (Klenow, Boehringer-Mannheim). This insert was ligated into the ApoE vector using the TaKaRA ligation kit. Insert orientation was checked by *Bam*HI digestion. The fragments which were digested by *Sal*I and *Eco*RI of these clones (ApoE-SLCO2B1-HCR.1tg) with correct insert orientation were purified by gel electrophoresis and dialysis, and then diluted to 3.5 ng/μl for pronuclear injection into fertilized FVB/NRj oocytes.

Intestine-specific expression of the human *SLCO2B1* cDNA was achieved by generating the following transgene constructs. An SV40 polyadenylation signal was released from pGL3 (Promega Corporation, Madison, WI) by digestion with *Xba*I and *Bam*HI and ligated into *Xba*I- and *Bam*HI-cut pSL1180 (American Pharmacia Biotech, Piscataway, NJ), yielding pSL1180-SV40. Human *SLCO2B1* cDNA was released as an *Xba*I/*Spe*I 2.2 kb fragment from pEF6/V5-HIS-TOPO-SLCO2B1, and ligated into the *Xba*I/*Spe*I sites of pSL1180-SV40. The SLCO2B1 open reading frame was cloned behind the murine villin promoter by PCR. In the first PCR, pEF6/V5-HIS-TOPO-SLCO2B1, a forward 5′-CCTCTAGGCTCGTCCACCATGGGACCCA-TAGGGCC-3′ primer with the last bases of the villin promotor and first bases of SLCO2B1 (including the ATG start codon) and a reverse 5′-CAGCCCC-GACGTCTGGCTGGAG-3′ primer aligning with SLCO2B1 sequence at its *Aat*II digestion site was used. Subsequently, the obtained PCR product was elongated at its 5′ villin promoter side using pKS-2kbVill as a template (kindly provided by Dr. D. Louvard, Institut Curie, Paris, France) containing the last 2 kb 3′ of the villin promoter [26]. This elongated product was used as the template for a subsequence at its *Afl*II digestion site, and the earlier reversed 5′-CAGCCCCGACGTCTGGCTGGAG-3′ primer, aligning with the SLCO2B1 sequence at its *Aat*II digestion site. Therefore, a PCR product was generated spanning the last part of the villin promoter sequence connected with the ATG start codon and subsequently the first part of SLCO2B1, flanked with *Afl*II and *Aat*II digestion sites. The *Afl*II- and *Aat*II-digested fragment was then inserted into the digested *Afl*II/*Aat*II site of the pKS-9kbVill containing the full murine villin promoter that stops at the *Aat*II site, yielding pKS-9kbVill-ATG-partial SLCO2B1. The right size of *Aat*II fragment (12.1 kb) released from pKS-9kbVill-ATG-partial SLCO2B1 was then inserted into the *Aat*II- and *Sca*I-digested pSL1180-SLCO2B1-SV40, yielding pKS-9kbVill-SLCO2B1-SV40. The *Bam*HI digestion site was used to check the insert orientation. A *Sal*I-*Sca*I excised insert of this clone was then purified and injected into pronuclei of FVB/NRj fertilized oocytes as described above.

Two-cell stage embryos were implanted into oviducts of pseudo-pregnant F1 fosters and carried to term. Transgenic founder lines were detected by initial PCR screen with forward 5′-CGCTTCGGCCTCTCC-3′ and reverse 5′-AAGGCTGTGTTCCCCACC-3′ primers to yield a 476 bp band. DNA was extracted from ear clips or tail tips of mice. Two independent founder lines were generated, and each was inbred to obtain homozygous lines as determined by quantitative PCR. Transgenic strains with either ApoE-promoter-driven liver-specific or villin-promoter-driven intestine-specific expression of human *SLCO2B1* were crossed to homozygosity into an *Slco1a/1b/2b1*$^{-/-}$ background, and the obtained strains were further referred to as Slco12B1-Apo and Slco12B1-Vil, respectively. Transgenic SLCO2B1 expression was monitored over minimally 4 generations and was found to be stable (data not shown).

2.5. Animals

Mice were housed and handled according to institutional guidelines complying with Dutch and EU legislation. All experimental animal protocols, including power calculations, designed under the nationally approved DEC/CCD project AVD301002016595 were evaluated and approved by the institutional animal care and use committee. Wild-type, *Slco1a/1b*$^{-/-}$, *Slco2b1*$^{-/-}$, *Slco1a/1b2/b1*$^{-/-}$, Slco12B1-Apo and Slco12B1-Vil mice, all of a > 99% FVB genetic background, were used between 9 and 16 weeks of age unless indicated otherwise. The animals were kept in a specific pathogen-free and temperature-controlled environment with a 12-hour light and 12-hour dark cycle, and they received a standard diet (Transbreed, SDS Diets, Technilab-BMI, Someren, The Netherlands) and acidified water *ad libitum*. Welfare-related assessments were carried out prior to, during, and after the experiments. Mice that showed discomfort levels higher than mild were humanely sacrificed.

2.6. Histological analysis

Tissues were fixed in 4% phosphate-buffered formalin, embedded in paraffin, sectioned at 4 μm, and stained with hematoxylin and eosin according to standard procedures. Immunohistochemistry on Slco12B1-Apo and Slco12B1-Vil tissues was conducted with a rabbit anti-human OATP2B1 polyclonal antibody (Bioss BS3913R) and secondary antibody conjugated to HRP-labeled polymers (ThermoFisher Scientific 31464).

2.7. Sampling for plasma clinical chemistry and RNA expression levels in liver, kidney, and small intestine

Blood was collected by cardiac puncture from wild-type, *Slco1a/1b*$^{-/-}$, *Slco2b1*$^{-/-}$, *Slco1a/1b/2b1*$^{-/-}$, Slco12B1-Apo and Slco12B1-Vil mice at 11–13 weeks (n = 6–9) in Eppendorf tubes (Hamburg, Germany) containing heparin as an anticoagulant. The mice were sacrificed by cervical dislocation, and selected tissues were rapidly collected. The small intestinal contents (SIC) were removed from small intestinal tissue (SI), which was rinsed with cold saline to remove any residual feces. Small pieces (~ 3 mm^3) of liver, kidney and SI were collected separately in a 2 ml Eppendorf tube (Hamburg, Germany) and immediately put on dry ice. Plasma was isolated from blood cells by centrifugation at 9000 × *g* for 6 min at 4 °C, then 100 μl was pipetted into brown Eppendorf tubes containing evaporated 1 μl ascorbate (100 mM) by SpeedVac SPD120 Vacuum Concentrator (Thermo Fisher Scientific, Waltham, Massachusetts), which was used to prevent oxidation of bilirubin. The rest of the plasma was used for other clinical chemistry parameter measurements. Tissue samples were sent to the Genomics Core Facility in our institute for RNA isolation and RNA sequencing analysis.

2.8. Determination of BMG, BDG, and UCB in plasma

The protocol was adapted from the method described by Spivak and Carey (1985) [27]. In brief, plasma samples were deproteinized with 2 volumes of MeOH after the addition of KOH (final concentration 5 μM). Following centrifugation for 2 min at 14,000 rpm, the supernatant was applied to a Pursuit C18, 5 μm, 3.0 × 100 mm HPLC column (Agilent Technologies, Amstelveen, The Netherlands). Starting eluent consisted of 50% MeOH/50% ammonium acetate (1% (w/v), pH = 4.5) (v/v), followed by a linear gradient to 100% MeOH in 20 min. Bilirubin was measured at the absorbance wavelength of 450 nm. Quantification of bilirubin monoglucuronide (BMG), bilirubin diglucuronide (BDG), and unconjugated bilirubin (UCB) was done by using a linear calibration curve of UCB, $1/X^2$ being the weighting factor. The detection limit was 0.05 μM for BMG, BDG, and UCB in plasma.

2.9. Clinical-chemical analysis of plasma

Standard clinical-chemical analyses on heparin plasma were performed on a Roche Hitachi 917 analyzer to determine levels of alkaline phosphatase, aspartate amino transaminase, alanine amino transaminase, γ-glutamyl transferase, lactate dehydrogenase, creatinine, urea, Na^+, K^+, Ca^{2+}, total protein, albumin, uric acid, cholesterol, and triglyceride.

2.10. RNA isolation and RNAseq analysis

RNA isolation from male mouse liver, kidney, and small intestine and subsequent RNA sequencing (RNA-seq) analysis were performed by the Genomics Core Facility in our institute (Supplemental Data). The isolated RNA from each organ in 6 mice of each mouse strain was pooled before RNA-seq analysis. The expression levels were checked and presented for the following mouse genes: *Slco1a1*, *Slco1a4–6*, *Slco1b2*, *Slco2b1*, *Slc10a1*, *Slc22a1–3*, *Slc22a6–10*, *Slc22a12*, *Abcc2–4*, *Abcb1a*, *Abcb1b*, *Abcg2*, *Aox1*, *Aox3*, *Ugt1a1*, and *Cyp3a*.

2.11. Plasma and tissue pharmacokinetic experiments

The stock solution of erlotinib was prepared in dimethyl sulfoxide (DMSO) at 10 mg/ml and diluted 100-fold with saline to reach 0.1 mg/ml of dosing solution. OSI-420 (desmethyl erlotinib) was first dissolved in DMSO at a concentration of 10 mg/ml, followed by 2-fold dilution with polysorbate 80/ethanol (1/1; v/v), and then further diluted with saline to obtain a dosing solution of 0.2 mg/ml. Final concentrations of solvents in the dosing solution were: 2%, 1%, 1%, and 96% (all v/v) for DMSO, polysorbate 80, ethanol, and saline, respectively. Pravastatin, fluvastatin and rosuvastatin were dissolved in saline at concentrations of 1, 1, and 0.5 mg/ml for oral administration at 10, 10, and 5 mg/kg to mice, respectively. Fexofenadine was first dissolved in DMSO at a concentration of 5 mg/ml, followed by 2-fold dilution with polysorbate 80/ethanol (1/1; v/v), and then further diluted with saline to obtain a dose solution of 0.1 mg/ml. Final concentrations of solvents in the dosing solution were: 2%, 1%, 1%, and 96% (all v/v) for DMSO, polysorbate 80, ethanol, and saline, respectively. All dosing solutions were freshly prepared on the day of experiment.

To minimize variation in absorption upon oral administration, mice were fasted for 2–3 h before one of the compounds was administered by gavage into the stomach at 10 μl/g body weight using a blunt-ended needle. Except for the pravastatin portal vein experiments, tail vein serial sampling was performed at indicated time points using heparinized capillary tubes (Sarstedt, Germany). At the last time points, 5 ml pipette tips were used to cover the snout of the mice, and they were deeply anesthetized with an isoflurane evaporator using 2–3% isoflurane together with 0.2 L/min air and 0.1 L/min oxygen forced flow. Cardiac puncture followed to collect blood in Eppendorf tubes (Hamburg, Germany) containing heparin as an anticoagulant. After sacrificing the anesthetized mice by cervical dislocation, selected tissues were rapidly collected. The small intestinal contents (SIC) were separated from small intestinal tissue (SI), which was rinsed with cold saline to remove any residual feces. Plasma was isolated from blood cells by centrifugation at 9000 × *g* for 6 min at 4 °C, and the plasma fraction was collected and stored at − 30 °C. Tissues were homogenized with appropriate amounts of ice-cold 4% (w/v) bovine serum albumin. All the samples were stored at − 30 °C until analysis.

2.12. LC-MS/MS analysis of drugs and metabolites

The concentrations of erlotinib and its metabolites [28], pravastatin [29], rosuvastatin, fluvastatin, and fexofenadine in plasma samples and tissue homogenates were measured using separate sensitive and specific liquid chromatography-tandem mass spectrometry methods (Supplemental Data). Assay validation studies performed with independently prepared quality control samples revealed that the within-day precision, between-day precision, accuracy and stability were in the range of current (FDA and EMA) bioanalytical requirements [30,31]. The range and type of calibration curves and the lower limit of quantification have been reported for each assay (Supplemental Material). Overall, the validation characteristics of all assays were considered to be acceptable for the purpose in all experiments with these compounds in the current study.

2.13. Pharmacokinetic calculations and statistical analysis

Pharmacokinetic parameters of compounds were calculated by a non-compartmental model using the PKSolver add-in program for Microsoft Excel [32]. The area under the curve (AUC) was calculated with the trapezoidal rule without extrapolating to infinity. Parameters like the peak plasma concentration (C_{max}) and time of peak plasma concentration (T_{max}) were estimated from the original data. Graphpad Prism 9 (Graphpad Software, La Jolla, CA) was used to plot the data, and

for the statistical analysis of all data sets. One-way analysis of variance (ANOVA) was used when multiple groups were compared, and the Bonferroni *post hoc* correction was applied to accommodate multiple testing. The two-sided unpaired student's *t* test was used when differences between two groups were assessed. When variances were not homogeneously distributed, data were first log-transformed before applying statistical analysis. Differences were considered statistically significant when $P < 0.05$. All data are presented as geometric mean ± SD. In order to clearly illustrate the functions of mOatp2b1 and hOATP2B1, we showed the results of some physiological and pharmacokinetic studies in knockout and humanized transgenic mice separately, even though they were performed at the same time. Of note, the statistical analyses and conclusions were confirmed not to be affected by this situation.

3. Results

3.1. Generation and characterization of Slco2b1 knockout and Slco1a/1b/2b1 cluster knockout mice

Slco2b1$^{-/-}$ mice were generated by deleting a genomic region containing exon 3 and the last nucleotides of exon 2 and replacing it with a reverse-oriented PGK-hygromycin-cassette, leading to a frameshift (Fig. 1A). Homozygous combination knockout mice lacking all *Slco1a/1b* and *Slco2b1* genes were obtained by crossing the previously described Slco1a/1b knockout mice [25] with Slco2b1 knockout mice. Disruption of the *Slco2b1* gene was confirmed by RT-PCR analysis as a sharp downregulation of Slco2b1 RNA levels in the liver and small intestine of single Slco2b1 and combination Slco1a/1b/2b1 knockout mice, in comparison with wild-type mice. In the kidney, this was not evident, probably due to the already very low expression of Slco2b1 in the wild-type kidney (Figs. 1B and 1C). Slco2b1 RNA expression in WT mice was much higher in liver than in small intestine and kidney (Fig. 1C). Although some truncated RNA was still detectable for the *Slco2b1* knockout allele, the engineered functional disruption of the coding region including a frameshift would preclude the formation of a functional Oatp2b1 protein.

Slco2b1$^{-/-}$ and *Slco1a/1b/2b1*$^{-/-}$ mice were viable and fertile and had normal life spans. Both male and female *Slco2b1*$^{-/-}$ and *Slco1a/1b/2b1*$^{-/-}$ mice at 9–16 weeks showed higher body weights than wild-type mice. Moreover, there was a significant increase in body weight of *Slco1a/1b/2b1*$^{-/-}$ compared to *Slco1a/1b*$^{-/-}$ mice (Fig. S2). No obvious abnormalities in tissues were observed in macro- and microscopic histological and pathological analysis in *Slco2b1*$^{-/-}$ and *Slco1a/1b/2b1*$^{-/-}$ mice at approximately 12 or 70 weeks of age. Clear jaundice due to hyperbilirubinemia was found in *Slco1a/1b/2b1*$^{-/-}$ mice, similar to that seen in *Slco1a/1b*$^{-/-}$ mice, but not in single *Slco2b1*$^{-/-}$ mice.

3.2. Expression levels of other detoxification proteins in tissues of Slco2b1$^{-/-}$ and Slco1a/1b/2b1$^{-/-}$ mice

The expression levels of various uptake and efflux transporters relevant for the disposition of drugs and many endogenous compounds, as well as some metabolizing enzymes in the liver, kidney, and small intestine of male wild-type, *Slco1a/1b*$^{-/-}$, *Slco2b1*$^{-/-}$, and *Slco1a/1b/2b1*$^{-/-}$ mice were determined by RNA-seq analysis (Table S1). Of note, in the small intestine, only *Slco2b1* was substantially expressed, but none of the *Slco1a/1b* genes. The expression of UDP-glucuronosyltransferase 1a1 (*Ugt1a1*) was assessed since it catalyzes the glucuronidation of bilirubin and pravastatin. Also, the expression of cytochrome P 450 3 A (*Cyp3a*) enzymes in the liver and intestine was included because these are important drug-metabolizing enzymes and participate in the oxidation of erlotinib to OSI-420 and OSI-413 [28,33]. Interestingly, the fairly low small intestinal RNA levels of *Ugt1a1* in wild-type mice were substantially upregulated (40- to 50-fold) in all the three knockout strains, and to levels as high as observed in the liver of all the strains. We also found that expression of *Cyp3a11*, the most highly expressed *Cyp3a* gene, was modestly reduced by around 2.2-, 1.3-, and 1.8-fold in the liver, and increased by around 2.6-, 2.3-, and 3.0-fold in the small intestine of *Slco1a/1b*$^{-/-}$, *Slco2b1*$^{-/-}$ and *Slco1a/1b/2b1*$^{-/-}$ mice, respectively, relative to wild-type mice. Although there was also a modest increase in the expression of *Cyp3a13* and *Cyp3a25* in the small intestine in the knockout strains, their absolute expression levels were relatively low. Of all other detoxification genes analyzed (other than *Slco1a/1b/2b1*), no substantial differences in expression were observed in *Slco2b1*$^{-/-}$ and *Slco1a/1b/2b1*$^{-/-}$ compared to wild-type mice. Furthermore, the expression of the analyzed genes was quite similar between *Slco1a/1b*$^{-/-}$ and *Slco1a/1b/2b1*$^{-/-}$ mice, except for *Slco2b1* in tested tissues (Table S1). Significantly, Slco2b1 was by far the most abundant Slco RNA detected in the small intestine, with the other *Slco1a/1b* genes hardly expressed; its intestinal levels were somewhat lower than those of Slco1a1 and Slco1b2 in the liver, and of Slco1a1 and Slco1a6 in the kidney.

3.3. Analysis of blood and plasma of Slco2b1$^{-/-}$ and Slco1a/1b/2b1$^{-/-}$ mice

Hematological examination of male and female *Slco2b1*$^{-/-}$ and *Slco1a/1b/2b1*$^{-/-}$ mice revealed no noticeable abnormalities. Using HPLC-MS/MS analysis of plasma bilirubin in male mice, *Slco2b1*$^{-/-}$ mice demonstrated an around 1.9-fold decrease in total bilirubin levels compared to wild-type mice ($P < 0.001$, Fig. 2A). This was mainly due to the reduced unconjugated bilirubin (UCB) in *Slco2b1*$^{-/-}$ mice (~2-fold, $P < 0.001$, Fig. 2D). Perhaps this might be related to the upregulated *Ugt1a1* in the intestine, aiding intestinal clearance of UCB. No significant differences were observed in bilirubin monoglucuronide (BMG) between wild-type and *Slco2b1*$^{-/-}$ mice. Bilirubin diglucuronide (BDG) was below the detection limit in both mouse strains. BMG was markedly increased by 1.45-fold, and BDG decreased by 1.21-fold in *Slco1a/1b/2b1*$^{-/-}$ compared to *Slco1a/1b*$^{-/-}$ mice, leading to a net 1.28-fold increase in total bilirubin levels (Figs. 2B and 2C). In contrast, in female mice, there were no significant differences in bilirubin levels between wild-type and *Slco2b1*$^{-/-}$ mice or between *Slco1a/1b*$^{-/-}$ and *Slco1a/1b/2b1*$^{-/-}$ mice (Fig. S3). Apart from this, no significant differences were found in other measured clinical chemistry parameters between wild-type and *Slco2b1*$^{-/-}$ mice. However, significantly increased levels of plasma LDL-cholesterol were observed when comparing *Slco1a/1b*$^{-/-}$ (2.9- and 2.0-fold for males and females, respectively) and *Slco1a/1b/2b1*$^{-/-}$ (3.5- and 2.2-fold for males and females, respectively) to wild-type mice (Table S2 and S3). Other measured clinical chemistry parameters were not different between these two mouse strains when considering both genders.

3.4. Roles of mouse Oatp2b1 in erlotinib and OSI-420 pharmacokinetics

In a recent positron emission tomography (PET) study, [^{11}C]erlotinib was suggested to be taken up into the liver by OATP2B1 [14]. To determine the role of the Oatp2b1 transporter in erlotinib disposition, 1 mg/kg erlotinib was administered orally to wild-type, *Slco1a/1b*$^{-/-}$, *Slco2b1*$^{-/-}$, and *Slco1a/1b/2b1*$^{-/-}$ mice. Levels of erlotinib and its two main metabolites, OSI-413 and OSI-420 (Fig. S1), were analyzed by LC-MS/MS. Plasma levels of erlotinib, OSI-420 and OSI-413 were not significantly different between single *Slco2b1*$^{-/-}$ and wild-type mice (Fig. S4). However, significantly reduced plasma exposure of OSI-420 and OSI-413, although not of erlotinib, was observed in *Slco1a/1b/2b1*$^{-/-}$ compared to *Slco1a/1b*$^{-/-}$ mice. This might suggest that Oatp2b1 normally facilitates intestinal re-absorption of OSI-420 and OSI-413 excreted through bile, increasing their availability. Based on these initial results, we directly administered OSI-420 at 2 mg/kg orally to the mice. As shown in Fig. 3, there was no significant difference in plasma AUC of OSI-420 between the wild-type and all knockout strains. However, the plasma exposure of OSI-420 was significantly reduced by

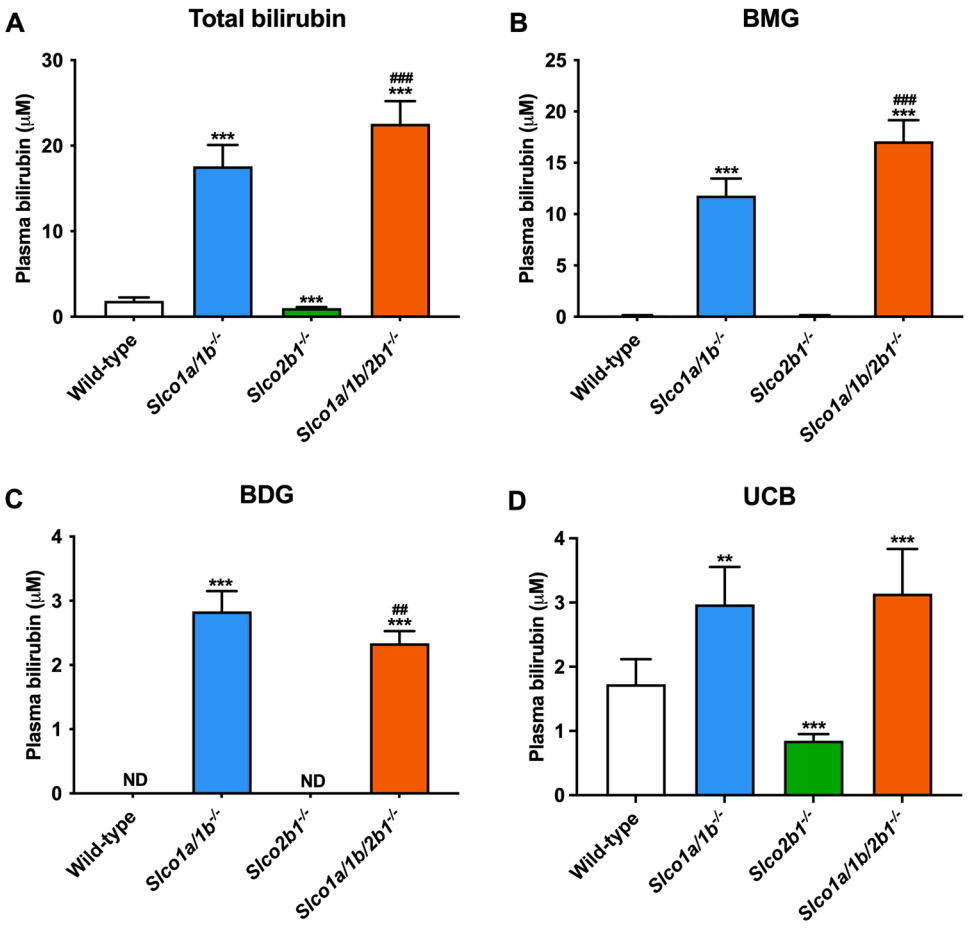

Fig. 2. Endogenous levels of total bilirubin (A), bilirubin monoglucuronide, BMG (B), bilirubin diglucuronide, BDG (C), and unconjugated bilirubin, UCB (D) in plasma of male wild-type, *Slco1a/1b*$^{-/-}$, *Slco2b1*$^{-/-}$, and *Slco1a/1b/2b1*$^{-/-}$ mice. Data are presented as mean ± SD (n = 6). *, $P < 0.05$; **, $P < 0.01$; ***, $P < 0.001$ compared to wild-type mice. $^{\#}$, $P < 0.05$; $^{\#\#}$, $P < 0.01$; $^{\#\#\#}$, $P < 0.001$ comparing *Slco1a/1b/2b1*$^{-/-}$ to *Slco1a/1b*$^{-/-}$ mice. ND, not detectable; detection limits were 0.05 μM.

2.5-fold in *Slco1a/1b/2b1*$^{-/-}$ compared to Slco1a/1b$^{-/-}$ mice. Unexpectedly, the small intestine tissue-to-plasma ratio of OSI-420 in *Slco1a/1b/2b1*$^{-/-}$ mice was significantly higher (2.7-fold, $P < 0.05$) rather than lower compared to *Slco1a/1b*$^{-/-}$ mice, whereas the absolute concentration was unchanged (Fig. 3E-F). This would perhaps suggest a role for Oatp2b1 in the basolateral efflux of OSI-420 from enterocytes into blood rather than in the apical uptake from the intestinal lumen. The OSI-420 small intestinal content as percentage of dose was not significantly different between *Slco1a/1b/2b1*$^{-/-}$ and Slco1a/1b$^{-/-}$ mice (data not shown). No significant and meaningful differences were observed among the other tested tissue distributions of OSI-420 between these strains, including the liver. Taking these two experiments together, it might suggest that intestinal Oatp2b1 could facilitate net intestinal absorption of OSI-420, boosting its oral availability, but perhaps primarily by mediating efflux across the basolateral membrane of enterocytes.

3.5. Roles of mouse Oatp2b1 in pravastatin pharmacokinetics

Keiser et al. (2017) reported that OATP2B1 can be localized in the basolateral membrane of the human jejunum, which might facilitate transport of pravastatin directly from blood towards the intestinal lumen [22]. To investigate the impact of the Oatp2b1 transporter on the pharmacokinetics of pravastatin, wild-type, *Slco1a/1b*$^{-/-}$, *Slco2b1*$^{-/-}$, and *Slco1a/1b/2b1*$^{-/-}$ mice received pravastatin orally at a dose of 10 mg/kg. Blood samples were collected from the portal vein and the general circulation (by cardiac puncture) to study the possible role of intestinal Oatp2b1 transporters in oral absorption of pravastatin. As shown in Fig. 4, no significant differences were observed in pravastatin exposure either in portal vein plasma or systemic plasma between wild-type and *Slco2b1*$^{-/-}$ mice. The pravastatin exposure in the portal vein was slightly increased by 1.6-fold in *Slco1a/1b*$^{-/-}$ mice, then substantially increased by 3.3-fold in the absence of Slco2b1 in *Slco1a/1b/2b1*$^{-/-}$ mice compared to wild-type mice. Moreover, the systemic exposure of pravastatin in *Slco1a/1b*$^{-/-}$ and *Slco1a/1b/2b1*$^{-/-}$ mice was markedly increased by 6.7-fold and 12.4-fold, respectively, relative to wild-type mice. These data suggest that Oatp2b1 could noticeably limit plasma exposure of oral pravastatin, but only when Oatp1a/1b was absent. Liver-to-plasma ratios (for either portal or systemic plasma) of pravastatin were similar between *Slco1a/1b*$^{-/-}$ and *Slco1a/1b/2b1*$^{-/-}$ mice and were both substantially lower than those in wild-type and *Slco2b1*$^{-/-}$ mice (Fig. 4G and H). The liver AUC of pravastatin was significantly 1.8-fold higher in *Slco1a/1b/2b1*$^{-/-}$ than in *Slco1a/1b*$^{-/-}$ mice (Fig. 4F), which was in line with the plasma pravastatin data. The reduced pravastatin liver concentrations due to the deficiency of Oatp1a/1b were markedly compensated by the increased plasma levels in mice further lacking Oatp2b1, probably because of the usually rapid equilibration between systemic plasma and liver levels of drugs. These results indicate that pravastatin hepatic uptake is substantially mediated by Oatp1a/1b transporters and that Oatp2b1 may also contribute to this process, perhaps especially when plasma pravastatin levels are low (Figs. 4G, 2h time point). Thus, Slco2b1 may limit the oral availability of pravastatin by helping to take it up in the liver, and perhaps by facilitating excretion into the small intestinal lumen.

3.6. Humanized mice with stable transgenic SLCO2B1 expression in liver or intestine of *Slco1a/1b/2b1*$^{-/-}$ mice

Human *SLCO2B1* transgenic mouse strains were generated using an ApoE promoter-HCR1 or a villin promoter-driven expression cassette

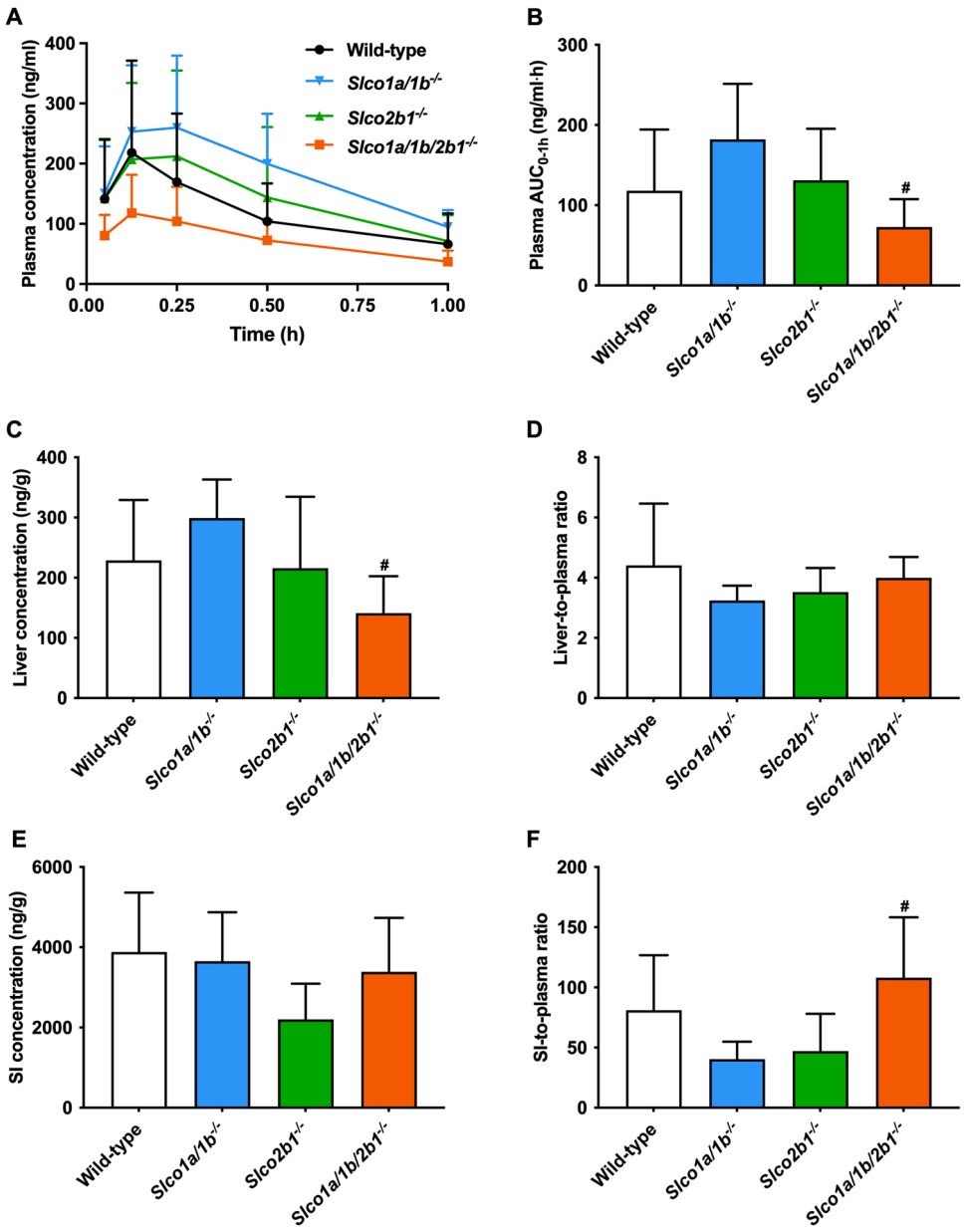

Fig. 3. OSI-420 systemic plasma concentration-time curves over 1 h (A), plasma $AUC_{0-1\ h}$ (B), and liver/small intestine (SI) tissue concentrations (C, E), and liver-, SI-to-plasma ratios (D, F) at 1 h in male wild-type, *Slco1a/1b*$^{-/-}$, *Slco2b1*$^{-/-}$, and *Slco1a/1b/2b1*$^{-/-}$ mice after oral administration of 2 mg/kg OSI-420. Data are presented as mean ± SD (n = 6). $^{\#}$, $P < 0.05$ comparing *Slco1a/1b/2b1*$^{-/-}$ to *Slco1a/1b*$^{-/-}$ mice.

containing human *SLCO2B1* cDNA (Figs. 5A and 5B), aiming primarily for protein expression in the liver or intestine, respectively. Since Oatp1a/1b transporters often play an important role in bilirubin and drug disposition, to eliminate any contributions from mOatp1a/1b and mOatp2b1 transporters, both transgenic strains were crossed into a *Slco1a/1b/2b1*$^{-/-}$ background and bred to homozygosity of knockout and transgene alleles. We named these mouse strains Slco1a/1b/2b1$^{-/-}$; Tg2B1Apo and Slco1a/1b/2b1$^{-/-}$;Tg2B1Vil, respectively. Both strains, abbreviated as Slco12B1-Apo and Slco12B1-Vil, respectively, were fertile and their life spans were not different from wild-type mice. However, both these transgenic strains showed similar body weights as *Slco1a/b/2b1*$^{-/-}$ mice, which are heavier than wild-type mice (Fig. S2). Hematological analysis of plasma and pathological analysis did not reveal obvious abnormalities in these strains. As shown in Tables S2 and S3, modestly but significantly higher plasma LDL-cholesterol levels were observed in Slco12B1-Apo mice compared to *Slco1a/1b/2b1*$^{-/-}$ mice, both in males and females. Higher overall cholesterol and HDL-cholesterol levels were only observed in female Slco12B1-Apo mice. In contrast, plasma total cholesterol, LDL- and HDL-cholesterol, and triglycerides were markedly reduced in male Slco12B1-Vil mice compared to *Slco1a/1b/2b1*$^{-/-}$ mice, reaching levels similar to those seen in wild-type mice. Other clinical-chemistry parameters were not much altered between these mouse strains.

Immunohistochemical staining of liver slides from Slco12B1-Apo mice showed that OATP2B1 protein expression was abundant at the basolateral (sinusoidal) membrane of hepatocytes (Fig. 5C), consistent with previous studies [7,10]. Basolateral positive staining was also observed in the epithelium of collecting ducts in the kidney in Slco12B1-Apo mice (Fig. 5D). Unexpectedly, the small intestine of Slco12B1-Vil mice displayed strong immunoreactivity of OATP2B1 in the basolateral membrane of enterocytes as evidenced by strong staining between adjacent enterocytes, with very little, if any, detectable signal in the apical membrane (Fig. 5F). In contrast, modest OATP2B1 staining was found locally in the apical or subapical region of enterocytes in

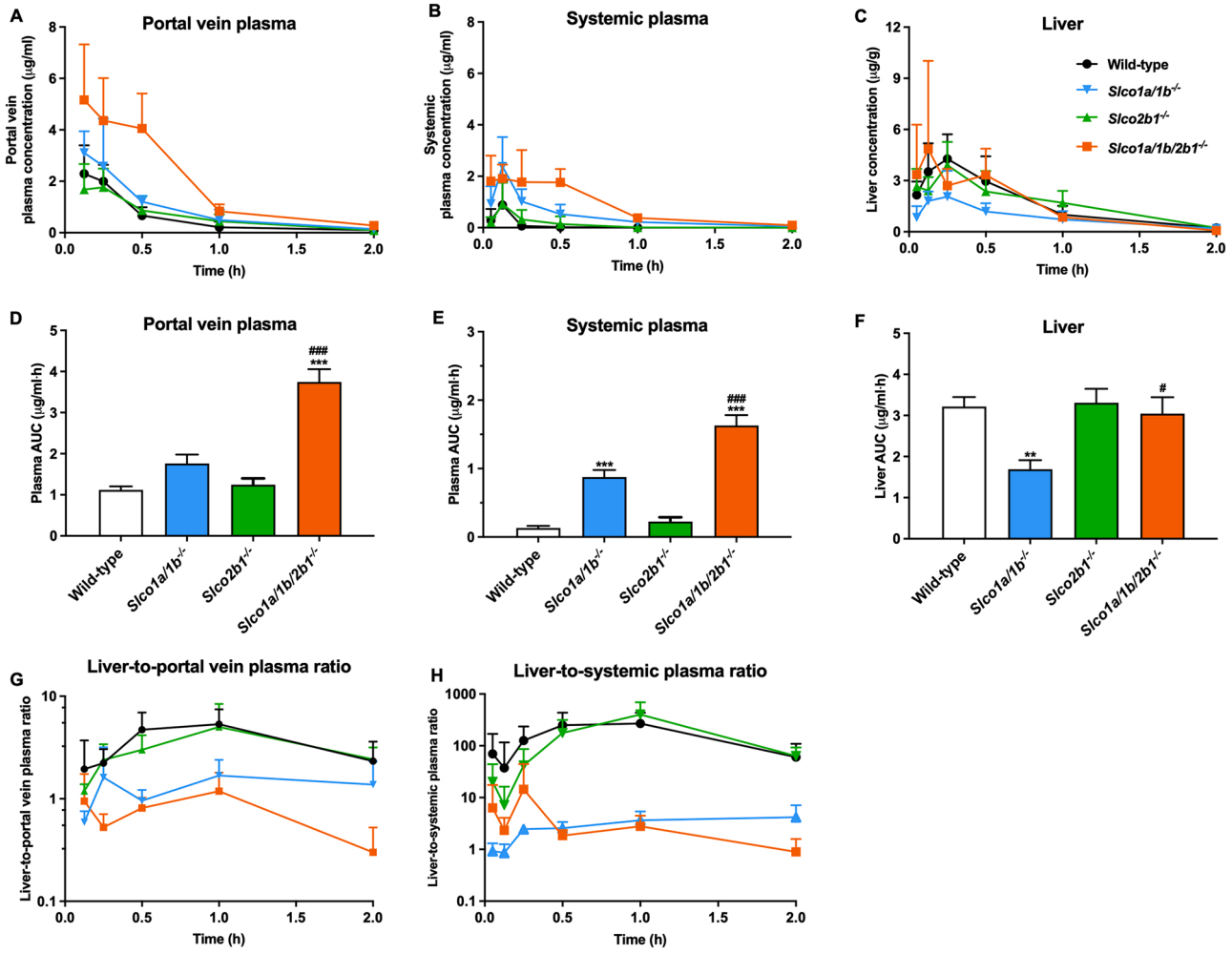

Fig. 4. Pravastatin portal vein plasma (A), systemic plasma (B), liver (C) concentration-time curves, and portal vein plasma (D), systemic plasma (E), and liver (F) $AUC_{0-2\,h}$, and liver-to-portal vein/systemic plasma ratio-time curves (G, H) over 2 h in male wild-type, *Slco1a/1b*$^{-/-}$, *Slco2b1*$^{-/-}$, and *Slco1a/1b/2b1*$^{-/-}$ mice after oral administration of 10 mg/kg pravastatin. Data are presented as mean ± SD (n = 5–13). * , $P < 0.05$; * *, $P < 0.01$; * ** , $P < 0.001$ compared to wild-type mice. $^{\#}$, $P < 0.05$; $^{\#\#}$, $P < 0.01$; $^{\#\#\#}$, $P < 0.001$ comparing *Slco1a/1b/2b1*$^{-/-}$ to *Slco1a/1b*$^{-/-}$ mice.

human small intestine, although staining was heterogeneous, sometimes also cytoplasmic, and not equally obvious in all parts of the intestinal epithelium (Fig. 5E).

The male, but not female, mice from both of the transgenic rescue strains displayed a substantial partial reversal of the increase in plasma BMG seen in *Slco1a/1b/2b1*$^{-/-}$ mice (Fig. 6 and Fig. S5). The BDG levels were markedly reduced only in male Slco12B1-Apo mice but not in Slco12B1-Vil mice. Of note, the modest (1.8- and 1.7-fold for males and females, respectively) increases in plasma UCB in *Slco1a/1b/2b1*$^{-/-}$ compared to wild-type mice were completely reversed in Slco12B1-Apo, and partially in Slco12B1-Vil mice in both genders, suggesting a significant role of human OATP2B1 in hepatic (and possibly intestinal) UCB uptake (Fig. 6D and Fig. S5D). Overall, the total bilirubin level was modestly but significantly reduced in the male transgenic mouse strains. Importantly, these results indicate transport functionality for both the hepatic and intestinal transgenic OATP2B1 transporter.

Like for the knockout strains, expression levels of various uptake and efflux transporters as well as metabolizing enzymes in the liver, kidney, and small intestine of male wild-type, *Slco1a/1b/2b1*$^{-/-}$, Slco12B1-Apo and Slco12B1-Vil mice were determined by RNA deep sequencing analysis. As shown in Supplemental Table 1, no substantial differences in expression levels of selected genes were observed for the humanized mouse strains compared to their control *Slco1a/1b/2b1*$^{-/-}$ strain.

3.7. Roles of human OATP2B1 protein in erlotinib and OSI-420 pharmacokinetics

To assess the possible interaction between human OATP2B1 and erlotinib *in vivo*, we performed a 4-h pharmacokinetic experiment using wild-type, *Slco1a/1b/2b*$^{-/-}$, Slco12B1-Apo, and Slco12B1-Vil mice. To avoid potential saturation of human OATP2B1 [14], we administered erlotinib orally to the mice at a low dose of 1 mg/kg. As shown in Fig. S6, plasma concentrations and exposure of erlotinib and OSI-413 in the transgenic strains were not significantly different from those in *Slco1a/1b/2b1*$^{-/-}$ mice. However, in Slco12B1-Apo mice, the plasma AUC of OSI-420 was reduced by 1.8-fold, and accordingly, its liver-to-plasma ratio substantially increased by 2.7-fold compared to *Slco1a/1b/2b1*$^{-/-}$ mice. This suggests that human OATP2B1 in the liver mediates hepatic uptake of OSI-420, thus reducing its availability. The substantially reduced OSI-420-to-erlotinib ratios in this strain (Fig. S6G) were in line with that assumption.

To further assess the impact of human OATP2B1 on the pharmacokinetics of OSI-420, we directly administered 2 mg/kg OSI-420 orally to mice. Again, plasma exposure of OSI-420 was significantly reduced in Slco12B1-Apo mice but not in Slco12B1-Vil mice, compared to *Slco1a/1b/2b1*$^{-/-}$ mice (Fig. 7). The liver-to-plasma and SI-to-plasma ratios of OSI-420 in Slco12B1-Apo were substantially increased compared to those in *Slco1a/1b/2b1*$^{-/-}$ mice. These results suggest that OATP2B1

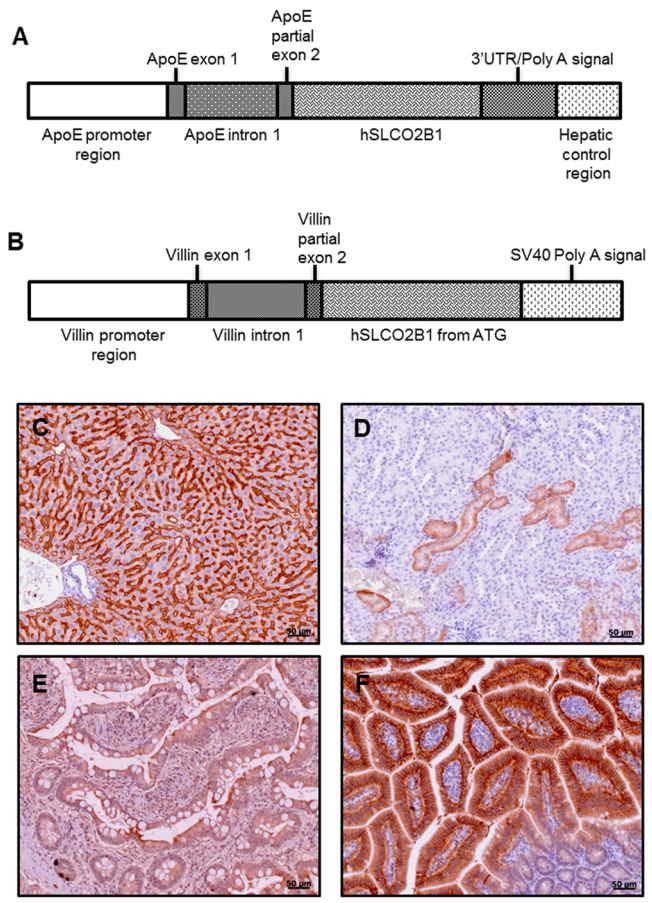

Fig. 5. Schematic structures of the ApoE promoter-HCR1-driven expression cassette (A) and the villin promotor-driven expression cassette (B) containing human SLCO2B1 cDNA. Immunohistochemical detection of human OATP2B1 protein in liver (C) and kidney (D) of Slco12B1-Apo transgenic mice. Immunohistochemical detection of human OATP2B1 transporter protein in human small intestine (E) and small intestine in Slco12B1-Vil transgenic mice (F). UTR, untranslated region.

could mediate hepatic uptake of OSI-420, limiting its oral availability and increasing its small intestine (content) distribution, presumably by facilitating biliary excretion (Fig. 7C-H).

3.8. Roles of human OATP2B1 protein in pravastatin pharmacokinetics

Earlier in this study, we observed markedly increased portal vein plasma exposure of pravastatin in *Slco1a/1b/2b1*$^{-/-}$ compared to *Slco1a/1b*$^{-/-}$ mice, which might suggest mouse Oatp2b1 at the basolateral membrane of enterocytes facilitates the intestinal re-excretion (back towards the intestinal lumen) of pravastatin, reducing the net oral absorption. This would be in addition to a role of Oatp2b1 in hepatic uptake of pravastatin. Given that human OATP2B1 protein was detected expressed in the basolateral side of enterocytes in our humanized transgenic Slco12B1-Vil mice, pravastatin might be a candidate substrate to study the functions of human OATP2B1 in the intestine. We therefore performed an experiment using wild-type, *Slco1a/1b/2b1*$^{-/-}$, Slco12B1-Apo, and Slco12B1-Vil mice. As shown in Fig. 8, after oral administration of 10 mg/kg pravastatin, plasma peak concentrations and plasma $AUC_{0-2\,h}$ of pravastatin were dramatically increased in *Slco1a/1b/2b1*$^{-/-}$ compared to wild-type mice. Moreover, the plasma exposure of pravastatin in Slco12B1-Apo and Slco12B1-Vil mice was markedly and significantly reduced compared to *Slco1a/1b/2b1*$^{-/-}$ mice and to similar levels. However, no significant differences in liver and small intestine distribution of pravastatin were observed between the transgenic and *Slco1a/1b/2b1*$^{-/-}$ strains, although the liver distribution was somewhat increased (1.7-fold, $P = 0.057$) in Slco12B1-Apo mice (Fig. 8C-F). Still, when correcting for the pravastatin plasma AUC, pravastatin accumulation was significantly increased in liver and intestine of Slco12B1-Apo compared to *Slco1a/1b/2b1*$^{-/-}$ mice (data not shown). The partial rescue of plasma exposure and limited rescue of liver and small intestine distribution of pravastatin in Slco12B1-Apo mice compared to *Slco1a/1b/2b1*$^{-/-}$ mice suggest that the absolute transport efficiency of pravastatin by human OATP2B1 was relatively modest. This is in line with a previous study, where the absolute uptake transport of pravastatin was far lower than that of rosuvastatin and fluvastatin in human OATP2B1-overexpressing HEK293 cells under the same conditions [34].

3.9. Roles of human OATP2B1 protein in rosuvastatin pharmacokinetics

Rosuvastatin has very low passive membrane permeability, and with limited metabolism, its disposition is mediated almost entirely by uptake and efflux transporters. Human OATP2B1, including both its major hepatic and intestinal protein variant, has been shown to transport rosuvastatin *in vitro* [35,36]. Moreover, pharmacokinetics and even lipid-lowering effects of rosuvastatin appeared to be affected by drug-drug interactions mediated by OATP2B1 and its genetic polymorphisms [37]. Yet, no significant changes were observed for rosuvastatin disposition in *Slco2b1*$^{-/-}$ C57BL/6 mice [24]. Consistent with this previous finding, we did not observe any significant differences in rosuvastatin pharmacokinetics either between wild-type and *Slco2b1*$^{-/-}$ mice, or between *Slco1a/1b/2b1*$^{-/-}$ and *Slco1a/1b*$^{-/-}$ mice (Fig. S7). However, in *Slco1a/1b/2b1*$^{-/-}$ mice, the plasma AUC was increased by 24.4-fold compared to wild-type and subsequently reduced by 3.8-fold and 2.5-fold upon transgenic overexpression of human *SLCO2B1* in liver (Slco12B1-Apo) or intestine (Slco12B1-Vil), respectively (Fig. 9B). As shown in Fig. 9A, the plasma concentrations of rosuvastatin were strongly reduced in Slco12B1-Apo mice at 3 and even 7.5 min after oral administration compared to those in *Slco1a/1b/2b1*$^{-/-}$ mice, but not in Slco12B1-Vil mice. This suggests that there was a marked first-pass effect in the liver in Slco12B1-Apo mice due to hepatic uptake of rosuvastatin mediated by OATP2B1. And hepatic overexpression of OATP2B1 in the transgenic mouse strain resulted in a substantial and highly significant, albeit partial, rescue of impaired liver distribution of rosuvastatin in *Slco1a/1b/2b1*$^{-/-}$ mice with liver-to-plasma ratios 1.9-fold increased (Fig. 9D). Intestinal overexpression of OATP2B1 in Slco12B1-Vil mice showed partial reversal of the reduced small intestine distribution of rosuvastatin, with SI-to-plasma levels 2.1-fold increased and (SIC % of dose)-to-plasma ratio 3.0-fold increased (Fig. 9F, H). This suggests a role of basolateral OATP2B1 in uptake of rosuvastatin from blood into the intestinal tissue. The increased small intestine (and its content) distribution of rosuvastatin in Slco12B1-Apo mice is most likely caused by increased biliary excretion as a consequence of increased hepatic uptake by human OATP2B1 (Fig. 9C-H). No meaningful and significant differences were observed in rosuvastatin distribution in other tested tissues, including brain, spleen, kidney, and testis (data not shown).

3.10. Roles of mouse and human OATP2B1 protein in fluvastatin and fexofenadine disposition

Two studies in a recently generated Oatp2b1-deficient mouse model in C57BL/6 background found that the plasma AUC and oral availability of fluvastatin and fexofenadine were reduced compared to those in wild-type mice [23,24]. This suggested that mouse Oatp2b1 may play a role in the intestinal absorption of these two compounds. To further investigate these findings, we performed analogous experiments by oral administration of fluvastatin (10 mg/kg) or fexofenadine (1 mg/kg) at the same dose as the previous studies, using our newly generated mouse models.

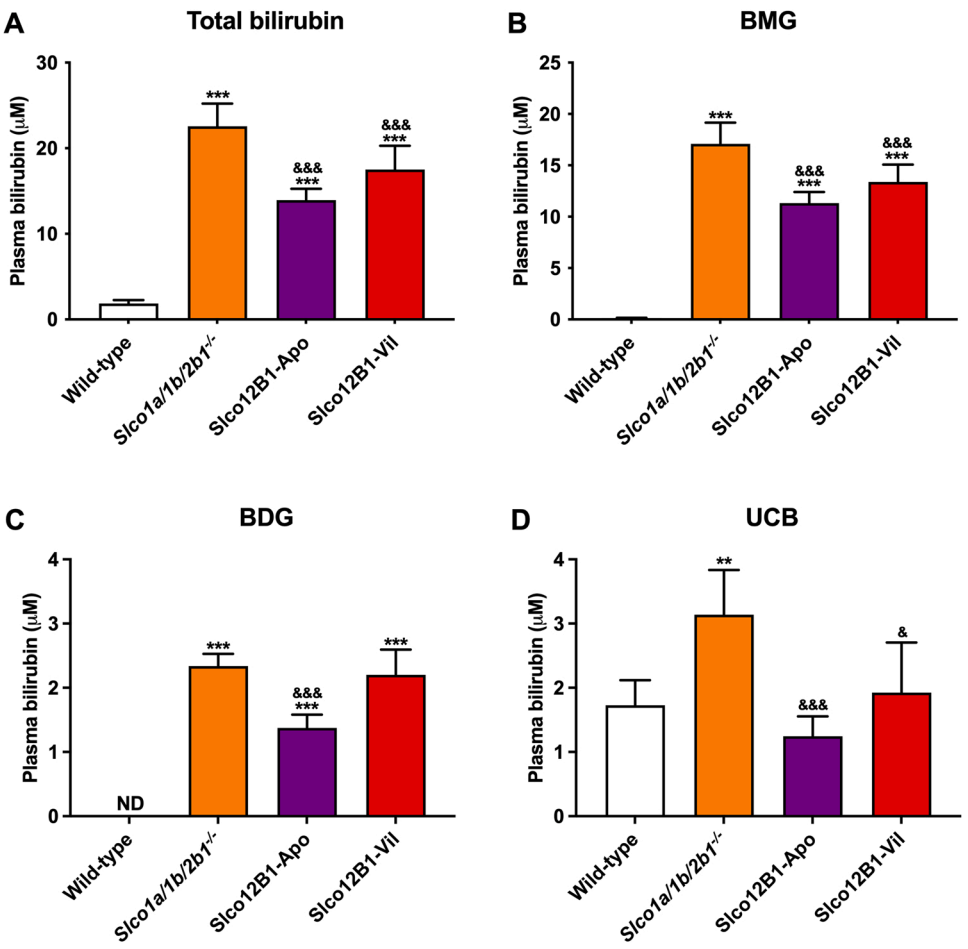

Fig. 6. Endogenous levels of total bilirubin (A), bilirubin monoglucuronide, BMG (B), bilirubin diglucuronide, BDG (C), and unconjugated bilirubin, UCB (D) in plasma of male wild-type, *Slco1a/1b/2b1*$^{-/-}$, Slco12B1-Apo, and Slco12B1-Vil mice. Data are presented as mean ± SD (n = 6). *, $P < 0.05$; **, $P < 0.01$; ***, $P < 0.001$ compared to wild-type mice. &, $P < 0.05$; &&, $P < 0.01$; &&&, $P < 0.001$ comparing Slco12B1-Apo and Slco12B1-Vil to *Slco1a/1b/2b1*$^{-/-}$ mice. ND, not detectable; detection limits were 0.05 μM. Note that wild-type and *Slco1a/1b/2b1*$^{-/-}$ data were also shown in Fig. 2.

As shown in Fig. 10, no significant differences were observed in fluvastatin pharmacokinetics between wild-type and *Slco2b1*$^{-/-}$ mice. Moreover, *Slco1a/1b*$^{-/-}$ and *Slco1a/1b/2b1*$^{-/-}$ mice behaved similarly in fluvastatin pharmacokinetics. These data clearly suggest that mouse Oatp2b1 plays little role in fluvastatin disposition, at least in the FVB/NRj background. The effect of removal of all mouse Oatp1a/1b/2b1 transporters on fluvastatin disposition, however, was very clear: plasma exposure over 2 h was 9.8-fold increased, liver-to-plasma ratio was 6.7-fold decreased, and SI-to-plasma ratio was 8.3-fold reduced compared to wild-type mice. Intriguingly, hepatic overexpression of human OATP2B1 in transgenic Slco12B1-Apo mice completely rescued the impaired liver uptake of fluvastatin, resulting in similar plasma and liver distribution levels as seen in wild-type mice (Fig. 10D). The oral availability and liver-to-plasma ratio of fluvastatin were not much affected by intestinal expression of human OATP2B1, but this did almost completely reverse the reduced small intestine (and its content) distribution (Fig. 10F-H). This suggests a role of the basolaterally expressed human OATP2B1 in intestinal uptake of fluvastatin from plasma (Fig. 10E-H). Again, in Slco12B1-Apo mice, the increased small intestinal fluvastatin levels likely reflect higher hepatobiliary excretion due to the higher liver fluvastatin levels. Finally, the modestly but significantly higher kidney distribution of fluvastatin in Slco12B1-Apo mice compared to *Slco1a/1b/2b1*$^{-/-}$ mice could be consistent with the immunohistochemistry data, suggesting that modest expression of human OATP2B1 may mediate uptake of fluvastatin into the kidney (Fig. S8).

Unexpectedly, significant changes in fexofenadine disposition were only found in both the Oatp1a/1b-deficient strains compared to wild-type mice but not in *Slco2b1*$^{-/-}$ mice (Fig. 11). Overexpression of human OATP2B1 in the liver and intestine could not significantly rescue any changes in *Slco1a/1b/2b1*$^{-/-}$ mice. These data suggest that neither mouse Oatp2b1 nor human OATP2B1 could substantially affect fexofenadine pharmacokinetics in these mouse models.

4. Discussion

Despite extensive *in vitro* transport characterization, there is still lack of clarity concerning the *in vivo* functions of hOATP2B1 and mOatp2b1. Although this study contributes a number of valuable insights, it does not definitively answer all outstanding questions. One reason for the challenge in assigning functions is the extensive overlap in substrate specificity and tissue distribution between OATP2B1/Oatp2b1 and other uptake transporters, including, but not limited to, the OATP1A/1B proteins. This has made it virtually impossible to find substrates that are sufficiently specific for direct *in vivo* studies of Oatp2b1 function. We have tried to ameliorate this situation by generating Oatp2b1 and Oatp1a/1b;Oatp2b1 combination knockout mice, but this was only partly successful due to remaining redundant functions likely of other transporters. An additional complication is the uncertain localization of mOatp2b1/hOATP2B1 in enterocytes (see also below).

To increase the chance of detecting certain pharmacokinetic functions, we tested a considerable range of known or suspected OATP2B1/Oatp2b1 substrate drugs. There are always many factors that can variably determine the pharmacokinetic behavior of individual drugs. Especially the possibility that each drug may be differently affected by other transporters (than OATP2B1/Oatp2b1), either uptake transporters or efflux transporters, or both, can affect the chance that clear functional transport by OATP2B1/Oatp2b1 can be detected *in vivo*. If there is extensive redundancy with other uptake transporters or a dominant counteracting effect of efflux transporters, it may be impossible to distinguish a specific contribution of OATP2B1/Oatp2b1. Below we

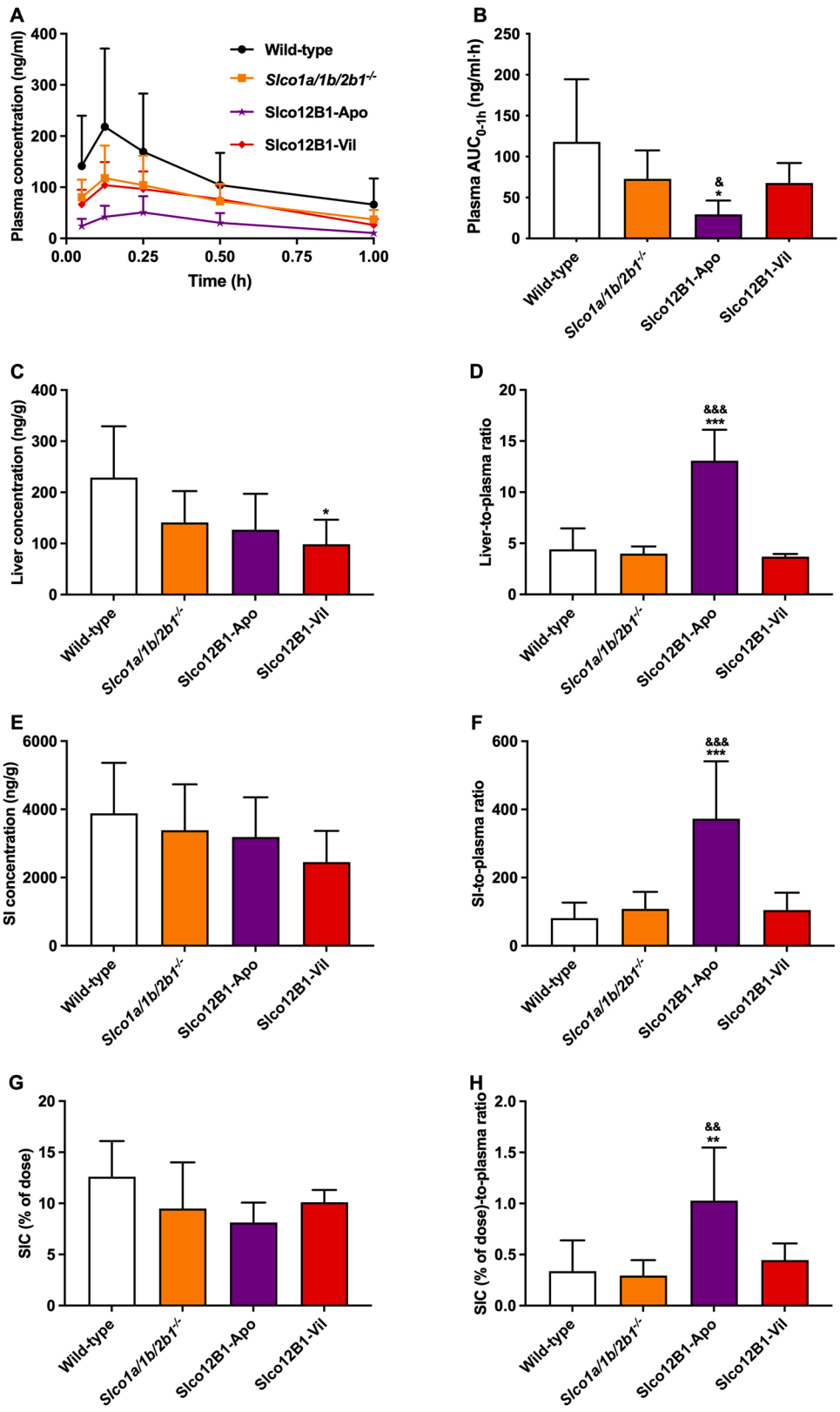

Fig. 7. OSI-420 systemic plasma concentration-time curves (A) over 1 h, plasma $AUC_{0-1\,h}$ (B), liver/small intestine (SI) concentrations (C, E), liver-, SI-to-plasma ratios (D, F), SIC (% of dose) (G), and SIC (% of dose)-to-plasma ratio (H) at 1 h in male wild-type, *Slco1a/1b/2b1*$^{-/-}$, Slco12B1-Apo, and Slco12B1-Vil mice after oral administration of 2 mg/kg OSI-420. Data are presented as mean ± SD (n = 6). SIC, small intestinal content. SIC (% of dose), drug percentage of dose in SIC expressed as total OSI-420 in SIC divided by total drug administered to the mouse. * , $P < 0.05$; * *, $P < 0.01$; * ** , $P < 0.001$ compared to wild-type mice. $^{\&}$, $P < 0.05$; $^{\&\&}$, $P < 0.01$; $^{\&\&\&}$, $P < 0.001$ comparing Slco12B1-Apo and Slco12B1-Vil to *Slco1a/1b/2b1*$^{-/-}$ mice. Note that wild-type and *Slco1a/1b/2b1*$^{-/-}$ data were also shown in Fig. 3.

briefly summarize the main findings from our pharmacokinetic studies.

Perhaps most strikingly, in spite of all the drugs tested, we found no convincing direct evidence that mOatp2b1, if indeed it is expressed in the apical membrane of enterocytes, can increase the oral availability of drugs. The compound that came closest was OSI-420, with a 2.5-fold reduced plasma AUC in *Slco1a/1b/2b1*$^{-/-}$ compared to *Slco1a/1b*$^{-/-}$ mice (Fig. 3). However, the simultaneous 2.7-fold relative increase in small intestinal tissue accumulation of OSI-420, instead of the expected decrease, did not support decreased uptake of the compound from the intestinal lumen. Apart from OSI-420, none of the other compounds

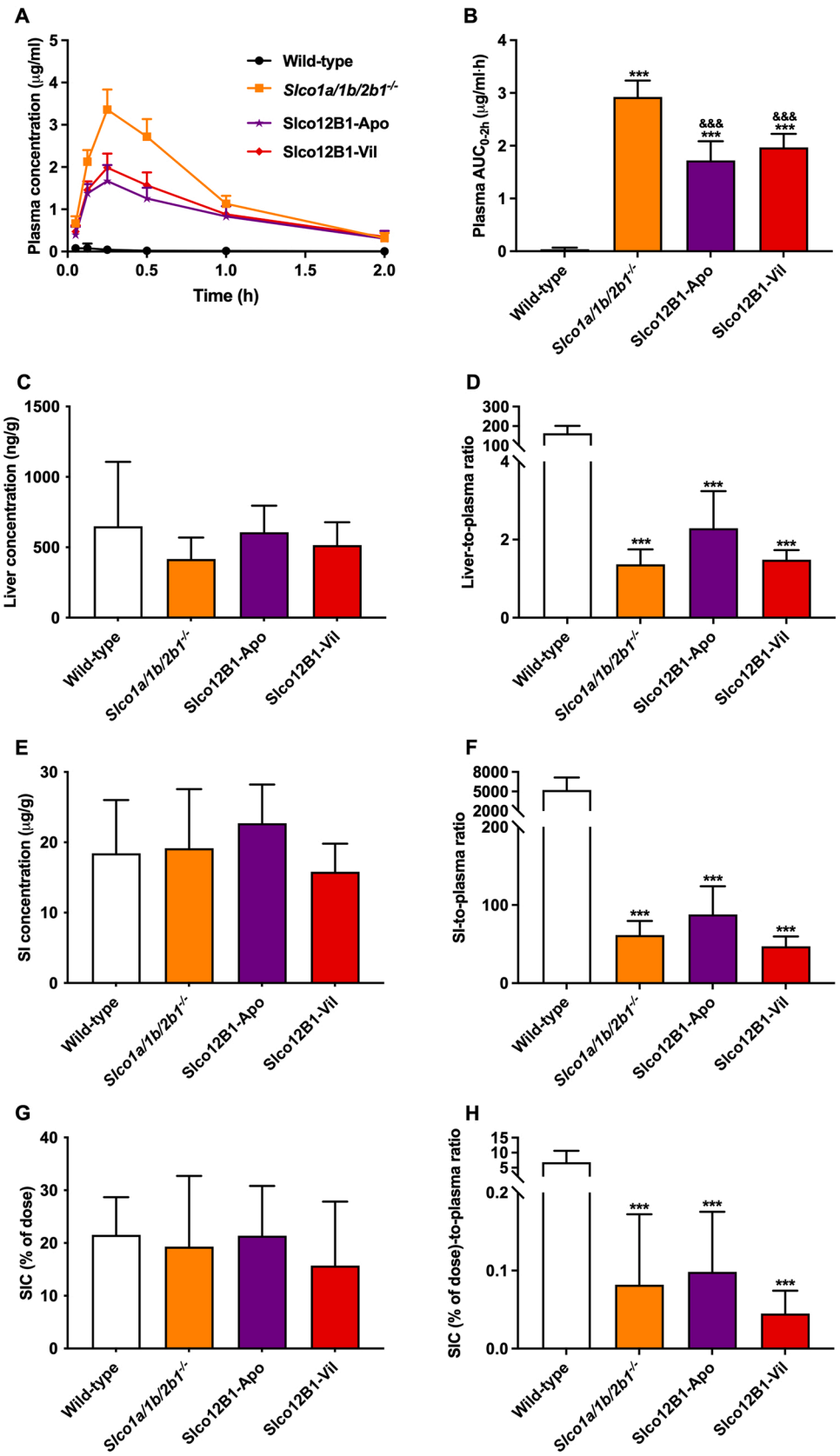

Fig. 8. Pravastatin systemic plasma concentration-time curves (A) over 2 h, plasma $AUC_{0-2\,h}$ (B), liver/small intestine (SI) concentrations (C, E), liver-, SI-to-plasma ratios (D, F), SIC (% of dose) (G), and SIC (% of dose)-to-plasma ratio (H) at 2 h in male wild-type, *Slco1a/1b/2b1*$^{-/-}$, Slco12B1-Apo, and Slco12B1-Vil mice after oral administration of 10 mg/kg pravastatin. Data are presented as mean ± SD (n = 5–6). SIC, small intestinal content. SIC (% of dose), drug percentage of dose in SIC expressed as total pravastatin in SIC divided by total drug administered to the mouse. *, $P < 0.05$; **, $P < 0.01$; ***, $P < 0.001$ compared to wild-type mice. &, $P < 0.05$; &&, $P < 0.01$; &&&, $P < 0.001$ comparing Slco12B1-Apo and Slco12B1-Vil to *Slco1a/1b/2b1*$^{-/-}$ mice. Note that wild-type and *Slco1a/1b/2b1*$^{-/-}$ data were also shown in Fig. 4.

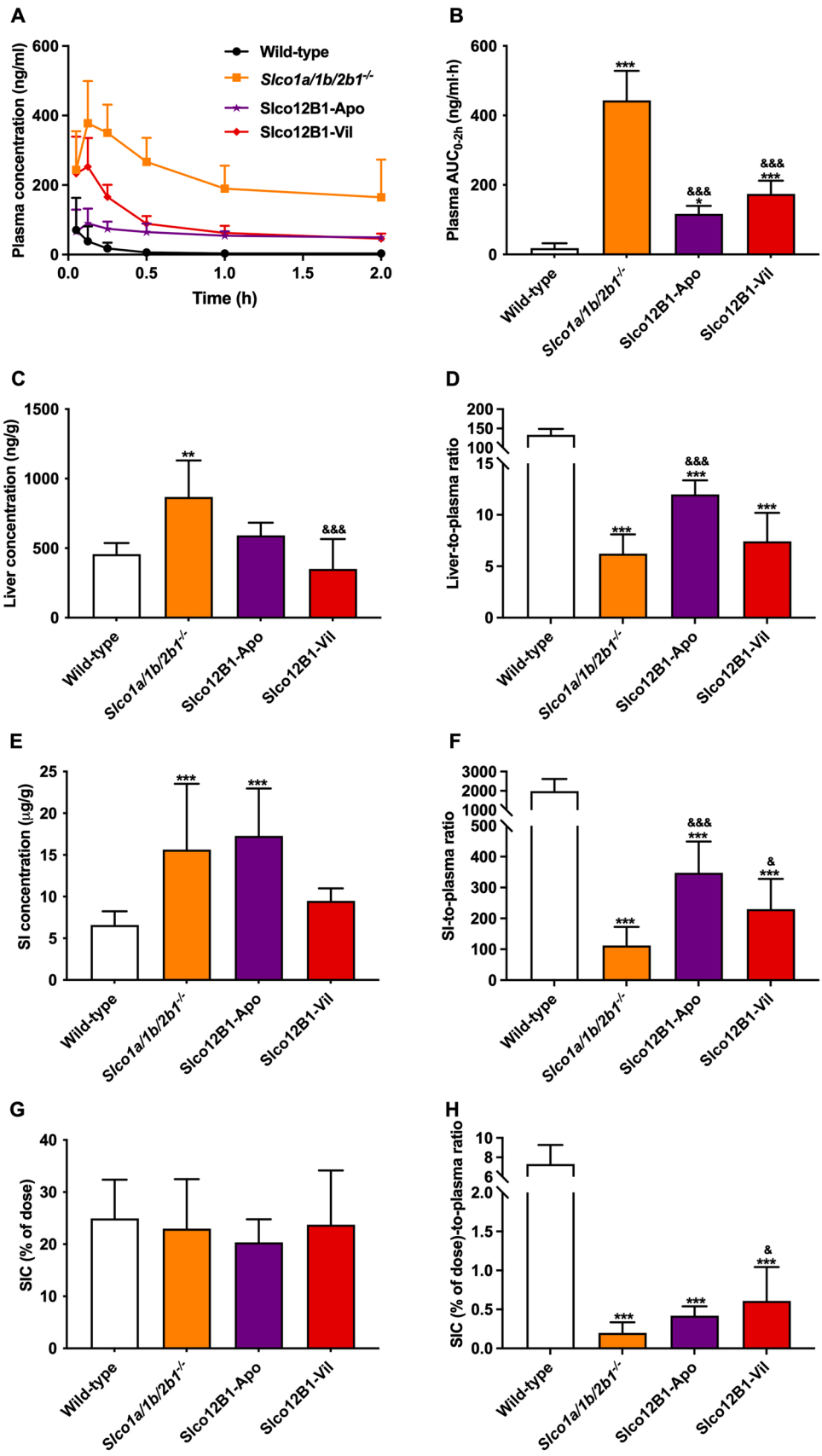

Fig. 9. Rosuvastatin systemic plasma concentration-time curves (A) over 2 h, plasma $AUC_{0-2\,h}$ (B), liver/small intestine (SI) concentrations (C, E), liver-, SI-to-plasma ratios (D, F), SIC (% of dose) (G), and SIC (% of dose)-to-plasma ratio (H) at 2 h in male wild-type, *Slco1a/1b/2b1*$^{-/-}$, Slco12B1-Apo, and Slco12B1-Vil mice after oral administration of 5 mg/kg rosuvastatin. Data are presented as mean ± SD (n = 6–10). SIC, small intestinal content. SIC (% of dose), drug percentage of dose in SIC expressed as total rosuvastatin in SIC divided by total drug administered to the mouse *, $P < 0.05$; **, $P < 0.01$; ***, $P < 0.001$ compared to wild-type mice. $^{\&}$, $P < 0.05$; $^{\&\&}$, $P < 0.01$; $^{\&\&\&}$, $P < 0.001$ comparing Slco12B1-Apo or Slco12B1-Vil to *Slco1a/1b/2b1*$^{-/-}$ mice.

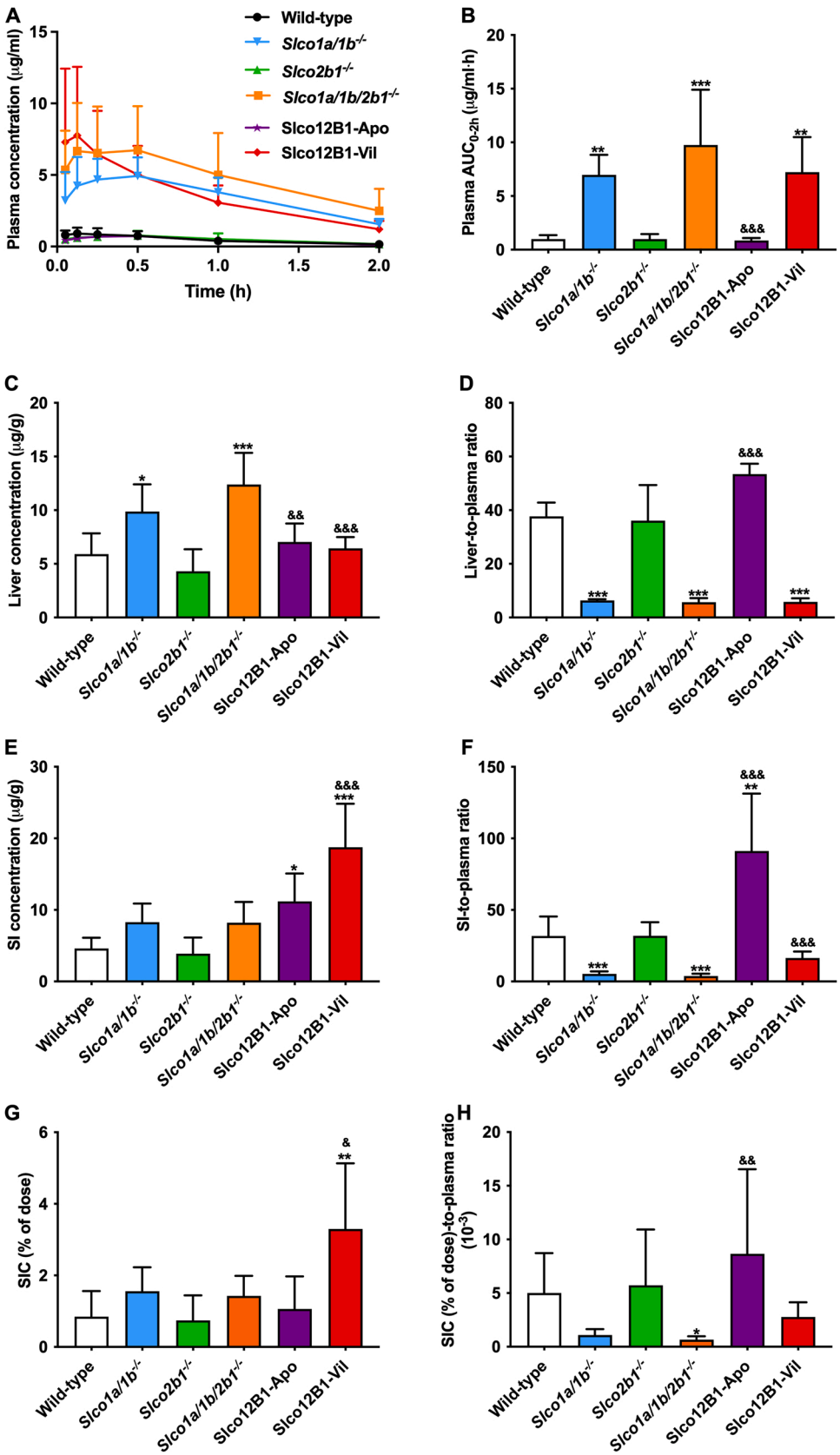

Fig. 10. Fluvastatin systemic plasma concentration-time curves (A) over 2 h, plasma $AUC_{0-2\,h}$ (B), liver/small intestine (SI) concentrations (C, E), liver-, SI-to-plasma ratios (D, F), SIC (% of dose) (G), and SIC (% of dose)-to-plasma ratio (H) at 2 h in male wild-type, *Slco1a/1b*$^{-/-}$, *Slco2b1*$^{-/-}$, *Slco1a/1b/2b1*$^{-/-}$, Slco12B1-Apo, and Slco12B1-Vil mice after oral administration of 10 mg/kg fluvastatin. Data are presented as mean ± SD (n = 6–7). SIC, small intestinal content. SIC (% of dose), drug percentage of dose in SIC expressed as total fluvastatin in SIC divided by total drug administered to the mouse. *, $P < 0.05$; * *, $P < 0.01$; * **, $P < 0.001$ compared to wild-type mice. $^{\&}$, $P < 0.05$; $^{\&\&}$, $P < 0.01$; $^{\&\&\&}$, $P < 0.001$ comparing Slco12B1-Apo and Slco12B1-Vil to *Slco1a/1b/2b1*$^{-/-}$ mice.

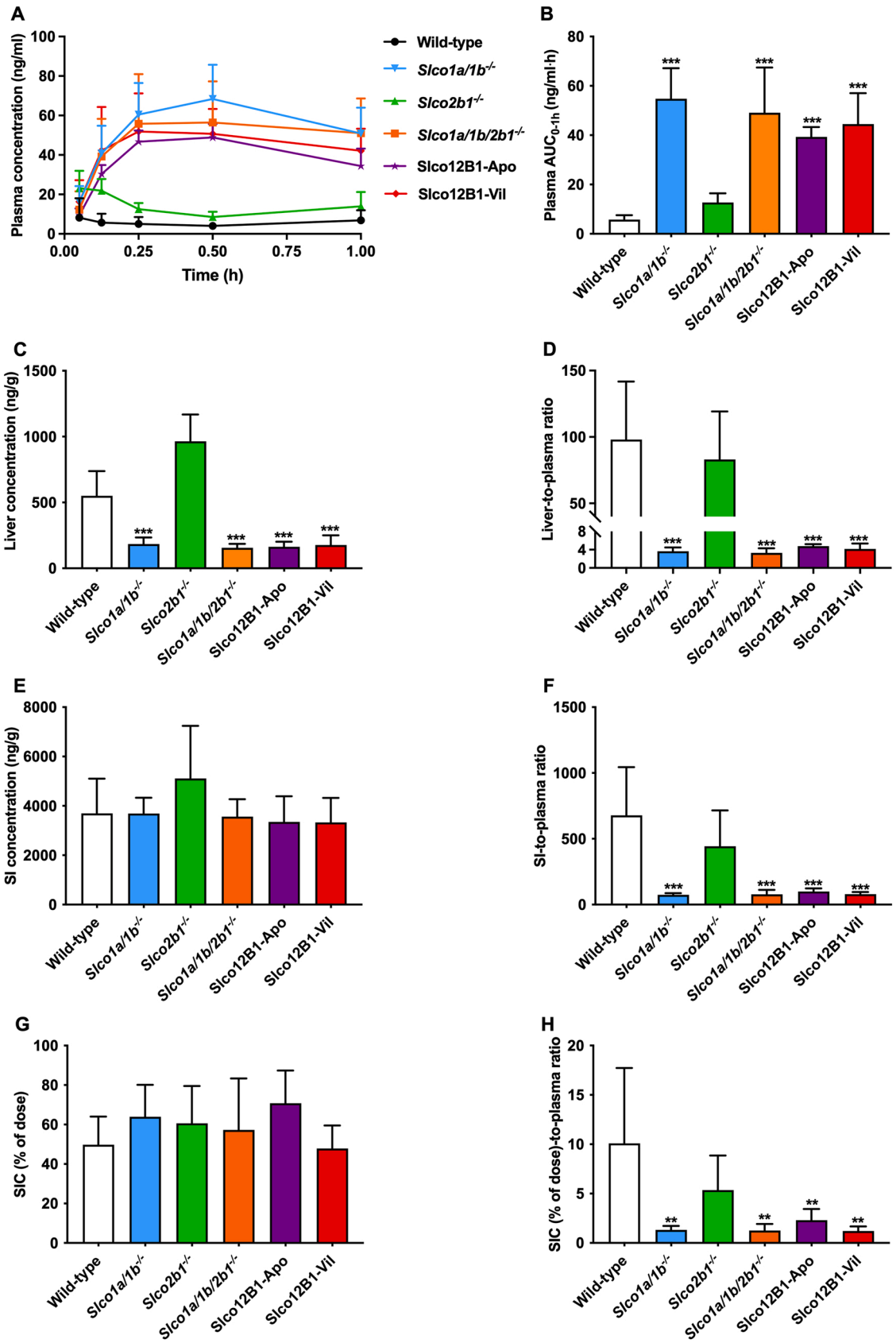

Fig. 11. Fexofenadine systemic plasma concentration-time curves over 1 h (A), plasma $AUC_{0-1\ h}$ (B), and liver/small intestine (SI) concentrations (C, E), liver-, SI-to-plasma ratios (D, F), SIC (% of dose) (G), and SIC (% of dose)-to-plasma ratio (H) at 1 h in male wild-type, *Slco1a/1b*$^{-/-}$, *Slco2b1*$^{-/-}$, *Slco1a/1b/2b1*$^{-/-}$, Slco12B1-Apo, and Slco12B1-Vil mice after oral administration of 1 mg/kg fexofenadine. Data are presented as mean ± SD (n = 6). SIC, small intestinal content. SIC (% of dose), drug percentage of dose in SIC expressed as total fexofenadine in SIC divided by total drug administered to the mouse. * , $P < 0.05$; * *, $P < 0.01$; * ** , $P < 0.001$ compared to wild-type mice.

tested (pravastatin, rosuvastatin, fluvastatin, fexofenadine) gave any indication for reduced oral availability upon ablation of mOatp2b1. Thus, collectively, it seems unlikely that intestinal mOatp2b1 as present in the FVB/NRj mouse strain can markedly contribute to the oral availability of most of its substrate drugs, even though its RNA level is substantial. However, we do not fully exclude that there may be circumstances for some drugs where such a contribution can be demonstrated.

In this context, it is worth noting that several Oatp transporters have been shown to be capable of bidirectional substrate transport, *e.g.* rat Oatp1a1, 1a4, and 1c1, and human OATP1B1 and 1B3 [38–41]. While for Oatp2b1/OATP2B1 this has not been directly investigated, given the structural homologies in the OATP1/2 families, basic transport mechanisms within this group are likely conserved. The possibility should thus be considered that under suitable circumstances, depending on the transport substrate and physicochemical gradient, Oatp2b1 may also mediate (or facilitate) cellular efflux of some drug substrates. In that case, mOatp2b1 located in the basolateral membrane of enterocytes could facilitate the net absorption of oral drugs across the intestinal epithelium by transporting the drug from the enterocyte lumen into blood. This could explain the behavior of OSI-420 as described in Fig. 3A and B, with 2.5-fold reduced plasma exposure of OSI-420 and 2.7-fold relative increase in intestinal tissue levels in *Slco1a/1b/2b1*$^{-/-}$ mice compared to *Slco1a/1b*$^{-/-}$ mice. However, detection of such a function would then be limited to mOatp2b1 and OSI-420, as we saw no indications for such effects with the other tested drugs or hOATP2B1.

We further found that hOATP2B1, but not mOatp2b1, can mediate hepatic uptake of OSI-420, whereas no function of basolateral intestinal hOATP2B1 for OSI-420 could be detected (Figs. 3 and 7). For pravastatin, liver mOatp2b1 and hOATP2B1 could modestly increase liver uptake, whereas basolateral intestinal hOATP2B1 could perhaps mediate some pravastatin clearance from plasma (Figs. 4 and 8). For rosuvastatin, no clear role of mOatp2b1 could be detected (Fig. S7), but hOATP2B1 could mediate marked hepatic uptake and also basolateral intestinal uptake and thus plasma clearance of rosuvastatin (Fig. 9). The latter results demonstrate that the basolateral hOATP2B1 in the small intestine (as well as in the liver) functions in rosuvastatin uptake from blood. For fluvastatin, whereas again no clear role for mOatp2b1 was observed, hOATP2B1 mediates extensive hepatic uptake and some basolateral intestinal uptake of fluvastatin, resulting in strongly increased hepatic plasma clearance (Fig. 10). Like for rosuvastatin, the results demonstrate functional uptake of fluvastatin by basolateral hOATP2B1 in the small intestine, even resulting in increased small intestinal content values. Finally, no significant pharmacokinetic effects were observed for oral fexofenadine.

Overall, while our results undoubtedly show that hepatic sinusoidal hOATP2B1 can contribute markedly to the hepatic uptake and thus plasma clearance of a number of drug substrates, we have not been able to test whether hOATP2B1, when expressed in the apical membrane of enterocytes, can enhance the oral availability of its substrates. This was because we did not obtain apical localization of hOATP2B1 in enterocytes of the villin transgenic mice. However, hOATP2B1, when expressed in the basolateral membrane of enterocytes (see also below), can contribute to the uptake of its drug substrates from blood and thus presumably their intestinal excretion and plasma clearance.

An important confounding factor in our studies is the uncertainty in the primary subcellular localization of OATP2B1 and Oatp2b1 in the small intestine. While some studies (including ours) find partly apparent apical or subapical, albeit modest and heterogeneous, localization of endogenous hOATP2B1 in human small intestinal enterocytes, other studies point to a predominantly basolateral localization (for instance, compare Kobayashi et al., 2003 and Keiser et al., 2017) [21,22]. Similar discrepant localization findings have been reported for the human intestinal Caco-2 cell line, with some studies reporting (sub-)apical localization and apparent function of OATP2B1 [8,42], and others basolateral [22], although this may also be due to subclonal variation in this cell line. However, when overexpressed in MDCK-II polarized canine kidney cells, hOATP2B1 consistently routes to the basolateral membrane [43,44], and also transgenic hOATP2B1 routed to the basolateral membrane in kidney proximal tubular epithelium (Fig. 5D). Furthermore, mOatp2b1 was primarily detected subapically in mouse small intestinal enterocytes but hardly or not in the apical plasma membrane [45,46]. The reason for these discrepancies is unclear. Perhaps physiological changes in the small intestine related to diet, fasting, local pH, stress, intestinal microbiome composition, or other factors can cause rerouting of OATP2B1 from basolateral or subapical membranes to the apical membrane of enterocytes. Our own work revealed similar discrepancies, as demonstrated in Fig. 5E and F: partly (sub)apical, albeit modest and heterogeneous, localization of endogenous human OATP2B1 in enterocytes and primarily basolateral localization of transgenic human OATP2B1 in mouse small intestine.

Considering all currently available immunohisto- and cytochemistry and biochemical data, the question may be raised whether OATP2B1 does not often localize primarily in the subapical region of human (and mouse) enterocytes, which may be mistaken for apical staining unless very high resolution and precise co-localization analyses are performed. In addition, often the enterocyte basolateral membrane may be the primary localization. For instance, Ferreira et al. (2018) presented highly heterogeneous OATP2B1 immunostaining in human small intestine, showing locally as much cytoplasmic and even basolateral staining as apical or subapical staining, but chose to only mention the apical (luminal) localization [47]. The actual observation, however, is well in line with the heterogeneous localization reported by Keiser et al., 2017, with mostly basolateral and occasionally (sub)-apical localization of OATP2B1 in the small intestine [22]. Likewise, Ferreira et al. (2018) reported apparent basolateral OATP2B1 staining in some parts of human kidney tubules, and apparent apical staining in other parts, although glomerular basolateral staining can perhaps not be excluded [47]. Again, this apparent apical staining may also have been subapical, as co-stained Pdzk1 was consistently detected more apically, resulting in very little direct overlap.

In this context, it is further worth noting that if OATP2B1/Oatp2b1 does indeed function as an apical intestinal uptake transporter of drugs, its effect on the systemic exposure of orally administered drugs would be opposed by its function in the liver: increased intestinal drug uptake would be counteracted by increased uptake into the liver, and thus presumably higher hepatic clearance. This also raises the question of the biological function of such a seemingly counterintuitive configuration. It might perhaps be relevant for compounds that need to be avidly taken up from the food and then preferentially routed into the liver, either for further biochemical processing or direct functioning inside the liver. However that may be, it may limit the possibility of detecting an impact of knocking out mOatp2b1, as decreased intestinal uptake of an oral drug might be offset by decreased hepatic clearance.

With respect to bilirubin homeostasis, there was a striking gender difference, with mOatp2b1 and hOATP2B1 having little impact on conjugated bilirubin disposition in females but a clear impact in males (Figs. 2 and 6 and Figs. S3 and S5). Perhaps female mice have a more prominent redundant conjugated bilirubin clearance or homeostasis mechanism than males, obscuring the OATP2B1/Oatp2b1 contribution. Nonetheless, in males, mOatp2b1 and hepatic and intestinal hOATP2B1 clearly contributed to the clearance of BMG and hepatic hOATP2B1 also of BDG (Figs. 2 and 6). Moreover, in males, both hepatic and intestinal hOATP2B1 increased UCB clearance (Fig. 6). Interestingly, the latter also applied in female mice, with significantly reduced UCB levels in both transgenic strains (Fig. S5). Collectively, the data indicate that mOatp2b1 can contribute to BMG clearance, whereas hOATP2B1 can contribute to UCB and BMG clearance in both liver and intestine, and in the liver to BDG clearance. The somewhat reduced UCB level observed in the male single *Slco2b1*$^{-/-}$ mice is perhaps a result of more extensive glucuronidation of bilirubin by the upregulated *Ugt1a1* gene in the small intestine (Table S1). Overall, the effects we observed on bilirubin

homeostasis in the different mouse strains (particularly in males) were in line with the effects we observed in the various pharmacokinetic studies. This suggests that the main impact of mOatp2b1 and hOATP2B1 on bilirubin homeostasis was primarily the result of altered clearance of UCB, BMG, and occasionally BDG.

Van de Steeg et al. (2012) showed that the hepatic transgenic expression of human OATP1B1 or OATP1B3 resulted in almost complete rescue of the Oatp1a/1b-knockout phenotype for conjugated bilirubin [48]. Still, we found that hOATP2B1 liver transgenic mice could also partially reverse the conjugated bilirubin increase in *Slco1a/1b/2b1*$^{-/-}$ mice. Of note, a virtually complete rescue of increased UCB levels in *Slco1a/1b/2b1*$^{-/-}$ mice was observed in mice expressing human OATP2B1 in the liver (Fig. 6). In contrast, human OATP1B1 and OATP1B3 appeared to play only a limited role in the UCB handling process [42]. These data suggest that human OATP2B1 might be a significant determinant for hepatic uptake of UCB while also contributing to the handling of glucuronidated bilirubin.

Except for the roles of OATP2B1 in bilirubin disposition, we found that the genetically modified mOatp2b1/hOATP2B1 mice showed generally similar increases in body weight compared to wild-type mice. This may suggest that loss of mOatp2b1 and/or mOatp1a/1b impaired the normal homeostasis of body weight, while overexpression of hOATP2B1 showed negligible rescue functions. However, intriguingly, the plasma LDL-cholesterol levels were significantly increased and decreased by hepatic and basolateral intestinal overexpression, respectively, of hOATP2B1 compared to their control mice. This may suggest that hOATP2B1 may participate in controlling lipid homeostasis *in vivo*. However, any underlying mechanisms should be further explored and clarified in the future.

Comparing with literature findings, we found some inconsistent and even contradictory observations in the present study. Chen et al. (2022) showed that genetic deletion or pharmacological inhibition of Oatp2b1 was associated with decreased absorption of fluvastatin by 2- to 3-fold in C57BL/6 J mice [23]. However, we did not observe any influence of mOatp2b1 in FVB/NRj mice at the same dose. Directly comparing data from these two studies, we found that the plasma concentration and AUC of fluvastatin in wild-type C57BL/6 J mice were much higher than FVB/NRj mice. This observation may highlight the potentially intrinsic differences in Oatp2b1 or other detoxification protein expression levels between two mouse strains. Of course, possible variations in experimental set-up between labs should also not be excluded. Moreover, the oral absorption but not plasma exposure of fexofenadine was found to the reduced in mOatp2b1 knockout C57BL/6 J mice. However, the relatively high variation of fexofenadine plasma concentrations and statistical analysis methods adopted in that study, using a large number of mice to document a modest effect, markedly weakened their conclusions. In our study, we did not observe any contribution of either mOatp2b1 or hOATP2B1 to fexofenadine pharmacokinetics. It should therefore be considered that conclusions about OATP2B1 functions might be affected by differences in other biological factors, even between two mouse strains.

As discussed above, there may be various reasons why drugs that are clear *in vitro* substrates of OATP2B1/Oatp2b1 do not show pronounced *in vivo* pharmacokinetic changes in the mouse models, especially with respect to intestinal disposition. Many different drugs and other compounds have been identified as OATP2B1 substrates *in vitro*. However, considering all the pharmacokinetic analyses we performed in our mouse OATP2B1 models, and the few borderline significant effects reported in the literature, we consider it very unlikely that mOatp2b1 and hOATP2B1 are major players in mediating the intestinal absorption of these compounds. This situation is further compounded by the apparently variable subcellular localization of OATP2B1 in enterocytes. This means that very likely other explanations will need to be found for some studies, often using fairly undefined fruit juice mixtures as Oatp2b1/OATP2B1 inhibitors, that suggested that OATP2B1 might be a major factor in mediating intestinal absorption of many drugs.

In conclusion, we have shown that single Oatp2b1 and combined Oatp1a/1b/2b1 knockout mice together present powerful tools in studying the roles of mOatp2b1 in liver physiology and drug pharmacokinetics by abrogating the substantial functional overlap with the mouse Oatp1a/1b transporters. Furthermore, the human OATP2B1 liver-specific transgenic mouse model represents a sensitive tool for screening *in vivo* substrates of hOATP2B1 and more importantly, a model to study the hepatic functions of OATP2B1. Also, while they have clear limitations for translational studies, transgenic mice expressing human OATP2B1 basolaterally in the intestine may still provide a tool for further understanding the role of OATP2B1 in the intestinal disposition of drugs. More work is required in this respect, including the need to rigorously establish the normal subcellular expression sites and functionality of human OATP2B1.

CRediT authorship contribution statement

Wenlong Li: Conceptualization, Methodology, Investigation, Data curation, Formal analysis, Writing – original draft. **Dilek Iusuf:** Conceptualization, Investigation, Data curation, Writing – review & editing. **Rolf W. Sparidans:** Investigation, Data Curation, Writing – review & editing. **Els Wagenaar:** Methodology, Investigation, Data curation. **Yaogeng Wang:** Investigation, Writing – review & editing. **Dirk R. de Waart:** Investigation, Data curation, Writing – review & editing. **Margarida L. F. Martins:** Investigation, Writing – review & editing. **Stéphanie van Hoppe:** Writing – review & editing. **Maria C. Lebre:** Resources, Writing – review & editing. **Olaf van Tellingen:** Investigation, Data curation, Writing – review & editing. **Jos H. Beijnen:** Supervision, Writing – review & editing. **Alfred H. Schinkel:** Supervision, Conceptualization, Project administration, Writing – review & editing.

Declaration of Competing Interest

The authors declare the following financial interests/personal relationships which may be considered as potential competing interests, Wenlong Li reports financial support was provided by China Scholarship Council. Yaogeng Wang reports financial support was provided by China Scholarship Council. Dilek Iusuf reports financial support was provided by Dutch Cancer Society. Margarida Martins reports financial support was provided by DiacetylM BV. Alfred Schinkel reports a relationship with Taconic Biosciences Inc that includes: funding grants.

Data Availability

Data will be made available on request.

Acknowledgements

This work was funded in part by the China Scholarship Council (to WL and YW), Dutch Cancer Society (to DI), and DiacetylM BV (to MM). We gratefully acknowledge the support from the Transgenic Facility and Genomic Core Facility of the Netherlands Cancer Institute in developing genetically modified mouse models and performing RNA sequencing analysis, respectively. We also thank Bart van Wijnen of the Clinical Chemistry lab at the Netherlands Cancer Institute for the clinical chemistry measurements of mouse plasma. We are further grateful for the support from the animal facility at the Netherlands Cancer Institute.

Appendix A. Supporting information

Supplementary data associated with this article can be found in the online version at doi:10.1016/j.phrs.2023.106724.

References

[1] B. Hagenbuch, P.J. Meier, Organic anion transporting polypeptides of the OATP/SLC21 family: phylogenetic classification as OATP/ SLCO superfamily, new nomenclature and molecular/functional properties, Pflug. Arch.: Eur. J. Physiol. 447 (5) (2004) 653–665.

[2] M. Niemi, Role of OATP transporters in the disposition of drugs, Pharmacogenomics 8 (7) (2007) 787–802.

[3] S. Durmus, S. van Hoppe, A.H. Schinkel, The impact of Organic Anion-Transporting Polypeptides (OATPs) on disposition and toxicity of antitumor drugs: insights from knockout and humanized mice, Drug Resist. Update.: Rev. Comment. Antimicrob. Anticancer Chemother. 27 (2016) 72–88.

[4] T. Nakanishi, I. Tamai, Genetic polymorphisms of OATP transporters and their impact on intestinal absorption and hepatic disposition of drugs, Drug Metab. Pharmacokinet. 27 (1) (2012) 106–121.

[5] D. Kovacsics, I. Patik, C. Ozvegy-Laczka, The role of organic anion transporting polypeptides in drug absorption, distribution, excretion and drug-drug interactions, Expert Opin. Drug Metab. Toxicol. 13 (4) (2017) 409–424.

[6] I. Tamai, J. Nezu, H. Uchino, Y. Sai, A. Oku, M. Shimane, et al., Molecular identification and characterization of novel members of the human organic anion transporter (OATP) family, Biochem Biophys. Res Commun. 273 (1) (2000) 251–260.

[7] G.A. Kullak-Ublick, M.G. Ismair, B. Stieger, L. Landmann, R. Huber, F. Pizzagalli, et al., Organic anion-transporting polypeptide B (OATP-B) and its functional comparison with three other OATPs of human liver, Gastroenterology 120 (2) (2001) 525–533.

[8] S.J. McFeely, L. Wu, T.K. Ritchie, J. Unadkat, Organic anion transporting polypeptide 2B1 - More than a glass-full of drug interactions, Pharm. Ther. 196 (2019) 204–215.

[9] H. Bronger, J. König, K. Kopplow, H.H. Steiner, R. Ahmadi, C. Herold-Mende, et al., ABCC drug efflux pumps and organic anion uptake transporters in human gliomas and the blood-tumor barrier, Cancer Res. 65 (24) (2005) 11419–11428.

[10] A. Obaidat, M. Roth, B. Hagenbuch, The expression and function of organic anion transporting polypeptides in normal tissues and in cancer, Annu Rev. Pharm. Toxicol. 52 (2012) 135–151.

[11] J. Matsumoto, N. Ariyoshi, M. Sakakibara, T. Nakanishi, Y. Okubo, N. Shiina, et al., Organic anion transporting polypeptide 2B1 expression correlates with uptake of estrone-3-sulfate and cell proliferation in estrogen receptor-positive breast cancer cells, Drug Metab. Pharmacokinet. 30 (2) (2015) 133–141.

[12] T. Nakano, S. Katsuki, M. Chen, J.L. Decano, A. Halu, L.H. Lee, et al., Uremic toxin indoxyl sulfate promotes proinflammatory macrophage activation via the interplay of OATP2B1 and Dll4-notch signaling, Circulation 139 (1) (2019) 78–96.

[13] E.B. Mougey, H. Feng, M. Castro, C.G. Irvin, J.J. Lima, Absorption of montelukast is transporter mediated: a common variant of OATP2B1 is associated with reduced plasma concentrations and poor response. Pharm. Genom. 19 (2) (2009) 129–138.

[14] M. Bauer, A. Matsuda, B. Wulkersdorfer, C. Philippe, A. Traxl, C. Ozvegy-Laczka, et al., Influence of OATPs on hepatic disposition of erlotinib measured with positron emission tomography, Clin. Pharmacol. Ther. 104 (1) (2018) 139–147.

[15] Y. Funai, Y. Shirasaka, M. Ishihara, M. Takemura, K. Ichijo, H. Kishimoto, et al., Effect of osmolality on the pharmacokinetic interaction between apple juice and atenolol in rats, Drug Metab. Dispos.: Biol. fate Chem. 47 (4) (2019) 386–391.

[16] T. Eley, T. Garimella, W. Li, R.J. Bertz, Asunaprevir: a review of preclinical and clinical pharmacokinetics and drug-drug interactions. Clin. Pharmacokinet. 54 (12) (2015) 1205–1222.

[17] T. Eley, Y.H. Han, S.P. Huang, B. He, W. Li, W. Bedford, et al., Organic anion transporting polypeptide-mediated transport of, and inhibition by, asunaprevir, an inhibitor of hepatitis C virus NS3 protease, Clin. Pharmacol. Ther. 97 (2) (2015) 159–166.

[18] J. Badée, B. Achour, A. Rostami-Hodjegan, A. Galetin, Meta-analysis of expression of hepatic organic anion-transporting polypeptide (OATP) transporters in cellular systems relative to human liver tissue, Drug Metab. Dispos.: Biol. fate Chem. 43 (4) (2015) 424–432.

[19] B. Prasad, A. Gaedigk, M. Vrana, R. Gaedigk, J.S. Leeder, L. Salphati, et al., Ontogeny of hepatic drug transporters as quantified by LC-MS/MS proteomics, Clin. Pharmacol. Ther. 100 (4) (2016) 362–370.

[20] A. Kalliokoski, M. Niemi, Impact of OATP transporters on pharmacokinetics, Br. J. Pharmacol. 158 (3) (2009) 693–705.

[21] D. Kobayashi, T. Nozawa, K. Imai, J. Nezu, A. Tsuji, I. Tamai, Involvement of human organic anion transporting polypeptide OATP-B (SLC21A9) in pH-dependent transport across intestinal apical membrane, J. Pharmacol. Exp. Ther. 306 (2) (2003) 703–708.

[22] M. Keiser, L. Kaltheuner, C. Wildberg, J. Müller, M. Grube, L.I. Partecke, et al., The organic anion-transporting peptide 2B1 is localized in the basolateral membrane of the human jejunum and Caco-2 monolayers, J. Pharm. Sci. 106 (9) (2017) 2657–2663.

[23] M. Chen, S. Hu, Y. Li, A.A. Gibson, Q. Fu, S.D. Baker, et al., Role of OATP2B1 in drug absorption and drug-drug interactions, Drug Metab. Dispos.: Biol. fate Chem. (2020).

[24] S. Medwid, M.M.J. Li, M.J. Knauer, K. Lin, S.E. Mansell, C.L. Schmerk, et al., Fexofenadine and rosuvastatin pharmacokinetics in mice with targeted disruption of organic anion transporting polypeptide 2B1, Drug Metab. Dispos.: Biol. fate Chem. 47 (8) (2019) 832–842.

[25] E. van de Steeg, E. Wagenaar, C.M. van der Kruijssen, J.E. Burggraaff, D.R. de Waart, R.P. Elferink, et al., Organic anion transporting polypeptide 1a/1b-knockout mice provide insights into hepatic handling of bilirubin, bile acids, and drugs, J. Clin. Investig. 120 (8) (2010) 2942–2952.

[26] D. Pinto, S. Robine, F. Jaisser, F.E. El Marjou, D. Louvard, Regulatory sequences of the mouse villin gene that efficiently drive transgenic expression in immature and differentiated epithelial cells of small and large intestines, J. Biol. Chem. 274 (10) (1999) 6476–6482.

[27] W. Spivak, M.C. Carey, Reverse-phase h.p.l.c. separation, quantification and preparation of bilirubin and its conjugates from native bile. Quantitative analysis of the intact tetrapyrroles based on h.p.l.c, their Ethyl. anthranilate azo Deriv. *Biochem. J.* 225 (3) (1985) 787–805.

[28] J.J.M. Rood, J.S. Toraño, V.J. Somovilla, J.H. Beijnen, R.W. Sparidans, Bioanalysis of erlotinib, its O-demethylated metabolites OSI-413 and OSI-420, and other metabolites by liquid chromatography-tandem mass spectrometry with additional ion mobility identification, J. Chromatogr. B, Anal. Technol. Biomed. life Sci. 1166 (2021), 122554.

[29] R.W. Sparidans, D. Iusuf, A.H. Schinkel, J.H. Schellens, J.H. Beijnen, Liquid chromatography-tandem mass spectrometric assay for pravastatin and two isomeric metabolites in mouse plasma and tissue homogenates, J. Chromatogr. B, Anal. Technol. Biomed. life Sci. 878 (28) (2010) 2751–2759.

[30] European Medicines Agency Guideline on Bioanalytical Method Validation 2022. https://www.ema.europa.eu/en/documents/scientific-guideline/ich-guideline-m10-bioanalytical-method-validation-step-5_en.pdf.

[31] Center for Drug Evaluation and Research of the U.S. Department of Health and Human Services Food and Drug Administration; Guidance for Industry; Bioanalytical Method Validation 2018. https://www.fda.gov/regulatory-information/search-fda-guidance-documents/bioanalytical-method-validation-guidance-industry.

[32] Y. Zhang, M. Huo, J. Zhou, S. Xie, PKSolver: An add-in program for pharmacokinetic and pharmacodynamic data analysis in Microsoft Excel. Comput. Methods Prog. Biomed. 99 (3) (2010) 306–314.

[33] N.F. Smith, S.D. Baker, F.J. Gonzalez, J.W. Harris, W.D. Figg, A. Sparreboom, Modulation of erlotinib pharmacokinetics in mice by a novel cytochrome P450 3A4 inhibitor, BAS 100, Br. J. Cancer 98 (10) (2008) 1630–1632.

[34] M.V. Varma, C.J. Rotter, J. Chupka, K.M. Whalen, D.B. Duignan, B. Feng, et al., pH-sensitive interaction of HMG-CoA reductase inhibitors (statins) with organic anion transporting polypeptide 2B1. Mol. Pharm. 8 (4) (2011) 1303–1313.

[35] R.H. Ho, R.G. Tirona, B.F. Leake, H. Glaeser, W. Lee, C.J. Lemke, et al., Drug and bile acid transporters in rosuvastatin hepatic uptake: function, expression, and pharmacogenetics, Gastroenterology 130 (6) (2006) 1793–1806.

[36] M.J. Knauer, A.J. Girdwood, R.B. Kim, R.G. Tirona, Transport function and transcriptional regulation of a liver-enriched human organic anion transporting polypeptide 2B1 transcriptional start site variant, Mol. Pharmacol. 83 (6) (2013) 1218–1228.

[37] T.E. Kim, D. Shin, N. Gu, B.H. Jung, J. Kim, Y.M. Cho, et al., The effect of genetic polymorphisms in SLCO2B1 on the lipid-lowering efficacy of rosuvastatin in healthy adults with elevated low-density lipoprotein, Basic Clin. Pharm. Toxicol. 121 (3) (2017) 195–201.

[38] L. Li, T.K. Lee, P.J. Meier, N. Ballatori, Identification of glutathione as a driving force and leukotriene C4 as a Substrate for oatp1, the hepatic sinusoidal organic solute transporter, J. Biol. Chem. 273 (26) (1998) 16184–16191.

[39] L. Li, P.J. Meier, N. Ballatori, Oatp2 mediates bidirectional organic solute transport: a role for intracellular glutathione, Mol. Pharmacol. 58 (2) (2000) 335–340.

[40] D. Sugiyama, et al., Functional characterization of rat brain-specific organic anion transporter (Oatp14) at the blood-brain barrier: high affinity transporter for thyroxine, J. Biol. Chem. 278 (44) (2003) 43489–43495.

[41] C. Mahagita, S.M. Grassl, P. Piyachaturawat, N. Ballatori, Human organic anion transporter 1B1 and 1B3 function as bidirectional carriers and do not mediate GSH-bile acid cotransport, Am. J. Physiol. -Gastrointest. Liver Physiol. 293 (1) (2007) G271–G278.

[42] Y. Sai, Y. Kaneko, S. Ito, K. Mitsuoka, Y. Kato, I. Tamai, et al., Predominant contribution of organic anion transporting polypeptide OATP-B (OATP2B1) to apical uptake of estrone-3-sulfate by human intestinal Caco-2 cells, Drug Metab. Dispos.: Biol. fate Chem. 34 (8) (2006) 1423–1431.

[43] K. Kopplow, K. Letschert, J. König, B. Walter, D. Keppler, Human hepatobiliary transport of organic anions analyzed by quadruple-transfected cells, Mol. Pharmacol. 68 (4) (2005) 1031–1038.

[44] K. Köck, A. Koenen, B. Giese, M. Fraunholz, K. May, W. Siegmund, et al., Rapid modulation of the organic anion transporting polypeptide 2B1 (OATP2B1, SLCO2B1) function by protein kinase C-mediated internalization, J. Biol. Chem. 285 (15) (2010) 11336–11347.

[45] T. Sugiura, T. Otake, T. Shimizu, T. Wakayama, D.L. Silver, R. Utsumi, et al., PDZK1 regulates organic anion transporting polypeptide Oatp1a in mouse small intestine, Drug Metab. Pharmacokinet. 25 (6) (2010) 588–598.

[46] T. Akazawa, Y. Uchida, M. Tachikawa, S. Ohtsuki, T. Terasaki, Quantitative targeted absolute proteomics of transporters and pharmacoproteomics-based reconstruction of P-glycoprotein function in mouse small intestine, Mol. Pharm. 13 (7) (2016) 2443–2456.

[47] C. Ferreira, P. Hagen, M. Stern, J. Hussner, U. Zimmermann, M. Grube, et al., The scaffold protein PDZK1 modulates expression and function of the organic anion transporting polypeptide 2B1, Eur. J. Pharm. Sci. 120 (2018) 181–190.

[48] E. van de Steeg, V. Stranecky, H. Hartmannova, L. Noskova, M. Hrebicek, E. Wagenaar, et al., Complete OATP1B1 and OATP1B3 deficiency causes human Rotor syndrome by interrupting conjugated bilirubin reuptake into the liver, J. Clin. Investig. 122 (2) (2012) 519–528.